# BRAIN
A JOURNAL OF NEUROLOGY

# Excitatory GABAergic signalling is associated with benzodiazepine resistance in status epilepticus

Richard J. Burman,[1,2,3] Joshua S. Selfe,[1] John Hamin Lee,[1] Maurits van den Berg,[1] Alexandru Calin,[3] Neela K. Codadu,[4] Rebecca Wright,[3] Sarah E. Newey,[3] R. Ryley Parrish,[4] Arieh A. Katz,[5] Jo M. Wilmshurst,[2] Colin J. Akerman,[3] Andrew J. Trevelyan[4] and Joseph V. Raimondo[1]

Status epilepticus is defined as a state of unrelenting seizure activity. Generalized convulsive status epilepticus is associated with a rapidly rising mortality rate, and thus constitutes a medical emergency. Benzodiazepines, which act as positive modulators of chloride ($Cl^-$) permeable $GABA_A$ receptors, are indicated as first-line treatment, but this is ineffective in many cases. We found that 48% of children presenting with status epilepticus were unresponsive to benzodiazepine treatment, and critically, that the duration of status epilepticus at the time of treatment is an important predictor of non-responsiveness. We therefore investigated the cellular mechanisms that underlie acquired benzodiazepine resistance, using rodent organotypic and acute brain slices. Removing $Mg^{2+}$ ions leads to an evolving pattern of epileptiform activity, and eventually to a persistent state of repetitive discharges that strongly resembles clinical EEG recordings of status epilepticus. We found that diazepam loses its antiseizure efficacy and conversely exacerbates epileptiform activity during this stage of status epilepticus-like activity. Interestingly, a low concentration of the barbiturate phenobarbital had a similar exacerbating effect on status epilepticus-like activity, while a high concentration of phenobarbital was effective at reducing or preventing epileptiform discharges. We then show that the persistent status epilepticus-like activity is associated with a reduction in $GABA_A$ receptor conductance and $Cl^-$ extrusion capability. We explored the effect on intraneuronal $Cl^-$ using both gramicidin, perforated-patch clamp recordings and $Cl^-$ imaging. This showed that during status epilepticus-like activity, reduced $Cl^-$ extrusion capacity was further exacerbated by activity-dependent $Cl^-$ loading, resulting in a persistently high intraneuronal $Cl^-$. Consistent with these results, we found that optogenetic stimulation of GABAergic interneurons in the status epilepticus-like state, actually enhanced epileptiform activity in a $GABA_A R$ dependent manner. Together our findings describe a novel potential mechanism underlying benzodiazepine-resistant status epilepticus, with relevance to how this life-threatening condition should be managed in the clinic.

1 Division of Cell Biology, Department of Human Biology, Neuroscience Institute and Institute of Infectious Disease and Molecular Medicine, Faculty of Health Sciences, University of Cape Town, Cape Town, 7925, South Africa
2 Department of Paediatric Neurology, Red Cross War Memorial Children's Hospital, Neuroscience Institute, University of Cape Town, Cape Town, 7700, South Africa
3 Department of Pharmacology, University of Oxford, Oxford, OX13QT, UK
4 Institute of Neuroscience, Medical School, Framlington Place, Newcastle upon Tyne, NE24HH, UK
5 Division of Medical Biochemistry, Department of Integrated Biomedical Sciences and Institute of Infectious Disease and Molecular Medicine, Faculty of Health Sciences, University of Cape Town, Cape Town, 7925, South Africa

Correspondence to: Joseph V. Raimondo
Department of Human Biology
University of Cape Town

Cape Town, Anzio Rd, 7925
South Africa
E-mail: joseph.raimondo@uct.ac.za

# Introduction

The majority of all spontaneously occurring seizures terminate within a few seconds to minutes and without medical intervention. When seizures fail to stop naturally, this is referred to as status epilepticus. This represents a neurological emergency and requires immediate therapeutic intervention. Convulsive status epilepticus occurs more frequently in children, and if not managed effectively, is associated with significant morbidity and even mortality (Boggs, 2004). Current first-line treatment for status epilepticus recommends the use of benzodiazepines (Glauser et al., 2016). These drugs work by positively modulating $Cl^-$-permeable ionotropic $GABA_A$ receptors ($GABA_AR$), which underlie the majority of fast inhibitory neurotransmission within the brain. The intent is to boost inhibitory signalling in an attempt to terminate status epilepticus. Unfortunately, benzodiazepine treatment fails to terminate seizures in a large fraction of patients, which underscores the inadequacy of our current first-line therapeutic strategy for treating this condition (Appleton et al., 2000; Mayer et al., 2002; Chin et al., 2008).

Current thinking in the field is that benzodiazepine resistance in status epilepticus is largely due to impaired $GABA_AR$ trafficking (Goodkin and Kapur, 2009). Both in vitro and in vivo animal models have shown that extended seizure activity is correlated with internalization of $GABA_ARs$ in the hippocampus (Kapur and Coulter, 1995; Goodkin et al., 2005; Naylor et al., 2005). In addition, status epilepticus has been shown to be associated with a reduction in surface expression of $GABA_AR$ subunits ($\gamma 2$), which are necessary for benzodiazepine binding (Goodkin et al., 2008). This line of reasoning suggests that status epilepticus-induced changes to the $GABA_AR$ impairs the ability of benzodiazepines to enhance the $GABA_AR$ conductance, thereby resulting in treatment failure.

It is well accepted that the intracellular concentration of $Cl^-$, and therefore the reversal potential for $GABA_ARs$ ($E_{GABA}$) can change over multiple time scales (Wright et al., 2011; Ellender et al., 2014; Sato et al., 2017). Long-term changes in the expression of $Cl^-$ transporter proteins modifies steady-state $E_{GABA}$ over development and in multiple disease states including epilepsy (Moore et al., 2017). In addition to these well-described long-term changes, short-term (seconds to minutes) changes in $E_{GABA}$ can occur following intense $GABA_A$ activation that causes $Cl^-$ influx, which can overwhelm $Cl^-$ extrusion mechanisms (Alger and Nicoll, 1979; Kaila et al., 1989; Staley et al., 1995; Wright et al., 2011). Furthermore, significant $Cl^-$ accumulation and a temporary excitatory shift in GABAergic signalling has been shown to accompany single seizure-like events in both in vitro (Lamsa and Kaila, 1997; Isomura et al., 2003; Fujiwara-Tsukamoto et al., 2010; Ilie et al., 2012; Ellender et al., 2014) and in vivo (Sato et al., 2017) models. The breakdown of the $Cl^-$ gradient serves to explain the surprising excitatory effects of GABAergic interneuronal subtypes recently observed during in vitro and in vivo seizure events (Ellender et al., 2014; Khoshkhoo et al., 2017; Magloire et al., 2019). This suggests that in circuits where seizures have caused sufficient $Cl^-$ loading, $GABA_AR$ mediated synaptic signalling can serve to exacerbate rather than control hyperexcitablity, which has direct relevance for the inhibitory efficacy of benzodiazepines. Deeb et al. (2013) have previously demonstrated that the benzodiazepine diazepam has reduced inhibitory capability under these conditions of activity-driven $Cl^-$ accumulation. However, it is currently unknown as to whether $Cl^-$ dynamics and seizure-associated shifts in GABAergic signalling are involved in the development of benzodiazepine resistance in status epilepticus.

In this study we combine clinical and experimental data to explore the phenomenon of benzodiazepine-resistant status epilepticus. First we document the incidence of benzodiazepine resistance in a South African cohort of paediatric patients in status epilepticus and provide clinical evidence that seizure duration prior to treatment is a useful predictor of benzodiazepine resistance. As status epilepticus is most often caused by acute brain insults resulting in sustained seizure-activity, we used the acute in vitro 0 $Mg^{2+}$ model of status epilepticus (Dreier et al., 1998) in both organotypic and acute brain slices to explore the cellular mechanisms underlying acquired benzodiazepine resistance. We demonstrate that the benzodiazepine diazepam loses its antiseizure efficacy and can actually enhance epileptiform discharges during status epilepticus-like activity. Similarly, we find that a low concentration of the barbiturate phenobarbital also exacerbates status epilepticus-like activity, while a high concentration of phenobarbital maintains an antiseizure effect. Using gramicidin perforated patch-clamp recordings, $Cl^-$ imaging and optogenetic control of GABAergic interneurons, we characterize changes in intracellular $Cl^-$ and GABAergic signalling during the development of status epilepticus. We find that although GABA-mediated conductances are reduced in early status epilepticus, pharmacoresistance is associated with deficits in $Cl^-$ extrusion capability and profound activity-dependent $Cl^-$ accumulation that results in excitatory interneuronal signalling via $GABA_ARs$.

# Materials and methods

## Clinical data

Clinical data were obtained from paediatric patients presenting with convulsive status epilepticus to the Red Cross War Memorial Children's Hospital (RCWMCH) from 2015 to 2018 as part of a clinical trial comparing second-line therapy for paediatric status epilepticus in a resource-limited setting. This study was approved by the University of Cape Town Human Ethics Committee (HREC 297/2005) and the study protocol was registered on the ClinicalTrials.gov registry (NCT03650270). The findings of this study have been published (Burman *et al.*, 2019). Convulsive status epilepticus was defined as any seizure that lasts longer than 5 min, or multiple discrete seizures between which there is no extended period of recovery between events (Trinka *et al.*, 2015). The onset of convulsive status epilepticus was taken as the time when the child caregiver or healthcare professional first documented clinical signs of a convulsive seizure. Upon admission, all patients were treated with benzodiazepines. If convulsive status epilepticus continued after two doses of benzodiazepines, patients were then given second-line therapy. A successful response to treatment was defined as a termination of signs of convulsive seizure activity. If a child did not respond to first-line treatment with benzodiazepines, they then received one of two second lines regimens. Study data were collected using a custom-made REDCap database (hosted by the University of Cape Town's eResearch Centre).

## Brain slice preparation

Slices were prepared from GAD2-cre-tdTomato mice (C57BL/6 background, JAX lab) or Wistar rats. The GAD2-cre-tdTomato strain is characterized by cre-recombinase and tdTomato expression in all GABAergic interneurons (Taniguchi *et al.*, 2011). The use of animals was approved by the University of Cape Town Animal Ethics Committee (mouse) or in accordance with regulations from the United Kingdom Home Office Animals (Scientific Procedures) Act (rat). Organotypic brain slices were prepared using 7-day-old animals and followed the protocol originally described by Stoppini *et al.* (1991) [for details see Raimondo *et al.* (2016)]. Recordings were performed 6–14 days post culture, which is equivalent to postnatal Days (P) 13 to 21. This and previous work has shown that pyramidal neurons in the organotypic hippocampal brain slice have mature and stable $Cl^-$ homeostasis mechanisms at this point, as evidenced by their hyperpolarizing $E_{GABA}$ (Ilie *et al.*, 2012; Raimondo *et al.*, 2012). For experiments using optogenetics, after 1 day in culture, slices prepared from GAD2-cre-tdTomato mice were transduced with adeno-associated vector serotype 1 (AAV1) containing a floxed-STOP channelrhodopsin (ChR2) linked to a yellow fluorescent protein (YFP), which resulted in selective expression of ChR2 in GABAergic interneurons (Royo *et al.*, 2008). For $Cl^-$ imaging experiments, neurons were biolistically transduced with ClopHensorN construct following the same procedure described by Raimondo *et al.* (2013). Acute brain slices were prepared from P14–P21 mice. Horizontal slices of the temporal lobe included the entorhinal cortex and hippocampal formation [as demonstrated in Mann *et al.* (2009) and shown in Supplementary Fig. 2].

## Electrophysiology

Brain slices were transferred to a submerged recording chamber (whole-cell and perforated patch experiments) or an interface recording chamber [local field potential (LFP) experiments] where they were continuously superfused with standard artificial CSF bubbled with carbogen gas (95% $O_2$: 5% $CO_2$) using peristaltic pumps (Watson-Marlow). The standard artificial CSF was composed of (in mM): NaCl (120); KCl (3); $MgCl_2$ (2); $CaCl_2$ (2); $NaH_2PO_4$ (1.2); $NaHCO_3$ (23); D-glucose (11) with pH adjusted to be between 7.35 and 7.40 using 0.1 mM NaOH. For patch-clamp experiments, neurons were visualized using a BX51WI upright microscope (Olympus) using $20\times$ or $40\times$ water-immersion objectives and targeted for recording. For whole-cell recordings, micropipettes were prepared from borosilicate glass capillaries (Warner Instruments) and filled with a low $Cl^-$ internal solution composed of (in mM): K-gluconate (120); KCl (10); $Na_2ATP$ (4); NaGTP (0.3); $Na_2$-phosphocreatinine (10) and HEPES (10). When recording GABAergic synaptic currents, pipettes were filled with a high $Cl^-$ internal solution ($Cl^-$ 141 mM) composed of (in mM): KCl (135), NaCl (8.9) and HEPES (10). Gramicidin perforated patch recordings (Kyrozis and Reichling, 1995) were performed using glass pipettes containing the high $Cl^-$ internal solution. Adequate perforation of the membrane was assessed by monitoring access resistance and was defined when access resistance was $<90$ M$\Omega$. Patch-clamp recordings were made with Axopatch 200B amplifiers (Molecular Devices) and data acquired using WinWCP (University of Strathclyde). LFP recordings were performed using an AC-coupled amplifier (A-M Systems). Data were acquired using the LabChart Pro (AD Instruments) with recordings processed using a 140 Hz low-pass filter. Seizure-like events (SLEs) were defined as events where significant deviations from the resting potential in LFP and patch-clamp recordings [$>2$ standard deviations (SD)] lasting at least 5 s. The late recurrent discharge (LRD) phase was defined as recurrent epileptiform discharges that persisted for at least 5 min. Slices that developed spontaneous SLEs prior to 0 $Mg^{2+}$ exposure were excluded from analysis to ensure that prior epileptiform activity would not have altered the neuronal network (Kamphuis *et al.*, 1991; Morimoto *et al.*, 2004). The following drugs were used: diazepam, flumazenil, CGP-35348, kynurenic acid, tetrodotoxin (TTX), QX-314 (Tocris) and phenobarbital (Aspen Pharmacare).

## Confocal imaging

A confocal microscope (Zeiss) was used to visualize tdTomato and YFP-labelled ChR2 expression using 561 nm and 488 nm lasers. ClopHensorN [modified from the original ClopHensor by Arosio *et al.* (2010)] expressing neurons were excited using 458, 488 and 561 nm lasers and emission collected by photomultiplier tubes (PMTs): between 500 and 550 nm for EGFP, and 635 and 700 nm for tdTomato. Calibration of the reporter and $Cl^-$ measurements were made as described previously (Raimondo *et al.*, 2013).

## Cell surface biotinylation and western blotting

Organotypic hippocampal slices were incubated for 3 h at 28–30°C, in either control artificial CSF or artificial CSF with 0 $Mg^{2+}$, while continuously bubbling with 95% $O_2$/5% $CO_2$. Biotinylation was performed to produce 'total' and 'surface' protein lysate samples as described in Wright *et al.* (2017). Blots were incubated with rabbit anti-C-terminus KCC2 (1:500, Merck Millipore) followed by horseradish peroxidase (HRP)-conjugated goat anti-rabbit antibody (1:2000, Thermo Scientific). For each sample, the surface protein was normalized against the total protein, which was run in the adjacent lane. As the ratio of surface/total was calculated within each sample, this controlled for differences in overall protein levels across samples and variance associated with loading.

## Data analysis

Clinical data were analysed using SPSS Statistics (IBM) while experimental data analysis was performed using MATLAB (MathWorks). Statistical measurements were performed using GraphPad Prism. Data are reported as either median with interquartile range (IQR) or mean ± standard error of the mean (SEM) unless otherwise stated.

## Data availability

All the data presented in this manuscript has been made publicly available and may be accessed using the following link: http://raimondolab.com/2019/09/08/awz283_data/.

# Results

## Benzodiazepine-resistance is associated with enhanced morbidity and can be predicted by seizure duration

A total of 144 admissions of paediatric convulsive status epilepticus from 111 patients were observed at RCWMCH between 2015 and 2018 (median age at admission 28.11 months IQR 15.5–66.1). Fifty-two per cent of admissions responded to first-line benzodiazepine treatment, typically lorazepam, diazepam or midazolam (termed 'benzodiazepine-sensitive'), while 48% did not (termed 'benzodiazepine-resistant') (Fig. 1A). We found no association between whether a patient had previously been admitted for seizures and benzodiazepine sensitivity, nor in whether they were previously diagnosed as having epilepsy (Supplementary Table 1). For patients admitted multiple times, we found no difference in benzodiazepine sensitivity (Supplementary Table 2). Benzodiazepine resistance was associated with enhanced morbidity as benzodiazepine-resistant patients required longer care in hospital (Fig. 1B) and were more likely to need admission to the paediatric intensive care unit (PICU, Fig. 1C). Whilst acute causes were the most

common precipitant of status epilepticus, we found no difference in the underlying aetiology between the groups (Fig. 1D). We found no significant difference between age at admission (Supplementary Table 3). Furthermore, we found no association between convulsive status epilepticus type, semiology or diagnosis of febrile status epilepticus and benzodiazepine sensitivity (Supplementary Table 3).

The median duration of status epilepticus prior to the time of initial treatment was 50.0 min (IQR 33.0–69.5), but notably, longer status epilepticus durations were increasingly associated with benzodiazepine resistance (Fig. 1E). These data suggested that the duration of status epilepticus at the time of admission could be a useful clinical classifier, especially since benzodiazepine resistance is associated with enhanced morbidity. We addressed this question using receiver operating characteristic (ROC) curve analysis (Fig. 1F), by assessing the relative proportions of true positive rates (short duration status epilepticus are benzodiazepine-sensitive; long duration status epilepticus are benzodiazepine-resistant) to false positive rates, as the classifier time changes from short (top right) to long (bottom left) durations. The area under curve (AUC) of 0.75 indicates that status epilepticus duration does indeed discriminate between these two patient populations, and importantly, it further indicates that the optimum discrimination threshold occurs at almost exactly 1 h (maximal deviation from the diagonal was at 61 min; Fig. 1E and F). A contingency table ('confusion matrix') using 1 h as the cut-off (Supplementary Table 4), shows that before this time, 67% of patients responded to benzodiazepine, but after that, only 18% did.

These clinical data suggest strongly that a critical factor is the continued seizure activity itself, and that the benzodiazepine resistance is an acquired, activity-dependent phenotype. There are striking parallels of pharmacoresistance, acquired over a similar time course, in acute rodent *in vitro* models, and so we used such a model to explore the underlying cellular mechanism.

## Early application of diazepam is antiseizure while late application enhances *in vitro* epileptiform activity

Our clinical data demonstrated a diverse set of causes for status epilepticus, and no particular set of causes of status epilepticus which enhanced the likelihood of benzodiazepine resistance. As acute brain insults (the most common cause in our clinical cohort) causing extended seizures lasting minutes to hours can result in benzodiazepine resistance, we used the well characterized *in vitro* 0 $Mg^{2+}$ model of acute seizures and status epilepticus (Anderson *et al.*, 1986; Mody *et al.*, 1987; Gutiérrez and Heinemann, 1999; Albus *et al.*, 2008). Here $Mg^{2+}$ removal from the artificial CSF, results in initial interictal-like activity followed by the gradual development of seizure-like events, which mimic what is observed in temporal lobe
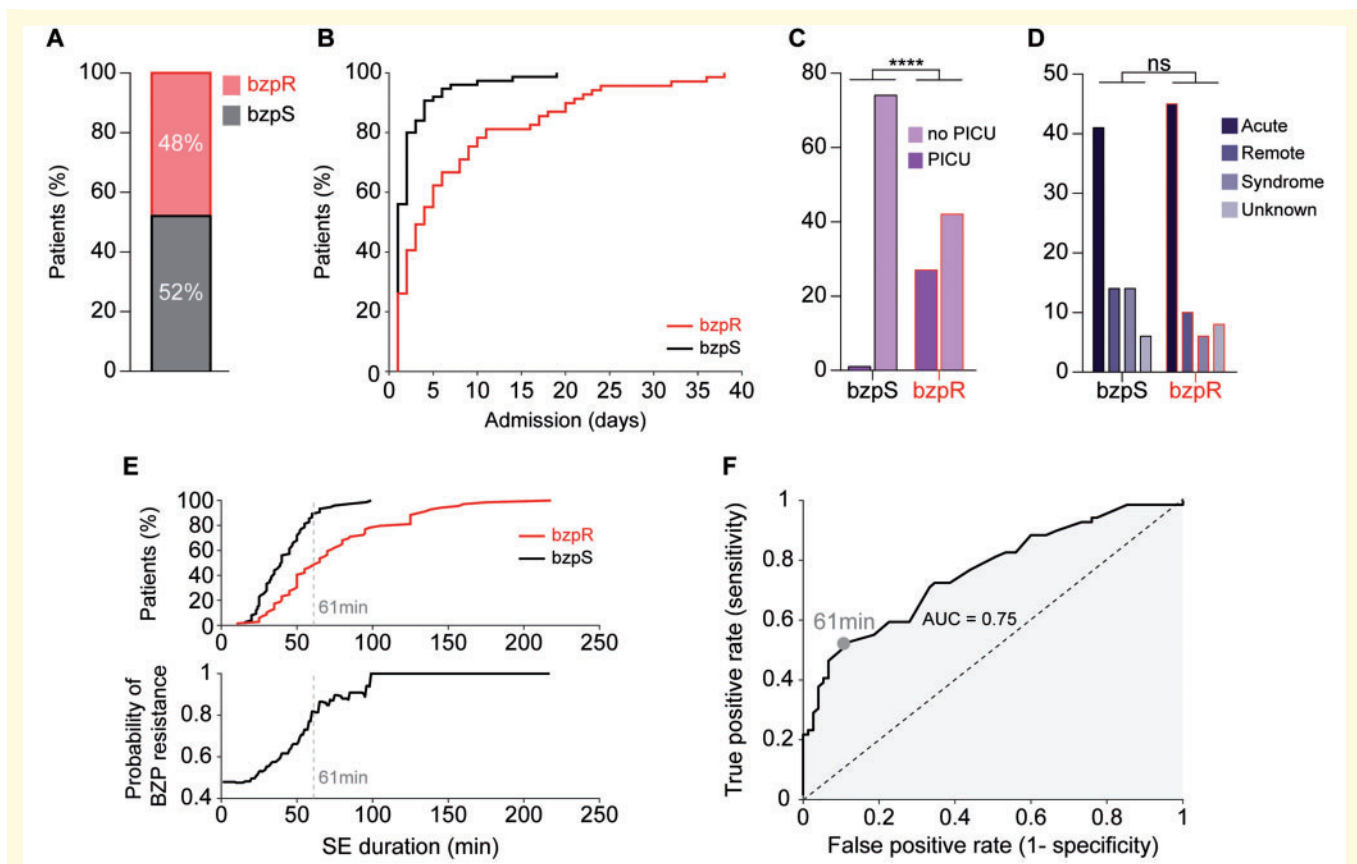
**Figure 1 Resistance to first-line benzodiazepine treatment increases with the duration of status epilepticus and is associated with increased morbidity.** (**A**) Proportion of paediatric patients presenting with convulsive status epilepticus (CSE) resistant (benzodiazepine-resistant, bzpR, red) or sensitive (benzodiazepine-sensitive, bzpS, black) to first-line treatment with benzodiazepines. (**B**) Benzodiazepine resistance was associated with longer hospital stays (benzodiazepine-sensitive: median 4.00 IQR 1.0–2.0 days versus benzodiazepine-resistant: median 4.0 days IQR 1.0–9.50 days, $P < 0.0001$, Mann-Whitney U-test) and (**C**) these patients were more likely to require admission to the paediatric intensive care unit [PICU, odds ratio (OR) = 47.57, 95% confidence interval (CI): 6.24–362.9, $P < 0.0001$, Fisher's exact test]. (**D**) There was no difference in underlying aetiology between the groups when dividing causes into four categories: 'Acute', acute illness; 'Remote', previous brain injury; 'Syndrome', established electroclinical syndrome; 'Unknown', no aetiology found during admission ($P = 0.25$, $\chi^2$ test). (**E**) *Top*: Cumulative frequency plot of benzodiazepine-resistant (red) and benzodiazepine-sensitive (black) patients as a function of seizure duration prior to treatment (benzodiazepine-resistant: median 40.0 IQR 28.0–52.0 min versus benzodiazepine-sensitive: median 65.00 IQR 45.0–95.0 min, $P < 0.0001$, Mann-Whitney U-test). *Bottom*: Increased status epilepticus duration is associated with enhanced probability of benzodiazepine resistance. The optimum discrimination threshold for separating benzodiazepine-resistant from benzodiazepine-sensitive patients calculated using data in **F** is indicated by the grey dashed line. (**F**) ROC curve analysing how well the status epilepticus duration classifies the likelihood of benzodiazepine sensitivity or resistance. *Top right* corresponds to short status epilepticus durations; *bottom left* to long status epilepticus durations. The maximal difference between the true and false positive rates occurs when the classifier is set at 61 min (grey circle).

seizures in humans (Anderson *et al.*, 1986; Dreier *et al.*, 1998). Importantly, after extended periods of $Mg^{2+}$ withdrawal, distinct ictal events no longer occur and are replaced by persistent seizure-like activity in the form of recurrent epileptiform discharges (Anderson *et al.*, 1986; Dreier *et al.*, 1998), which strongly resemble clinical EEG recordings of convulsive status epilepticus (Fig. 2A). This late-stage activity is also referred to as the LRD phase and represents the best available *in vitro* model of status epilepticus (Zhang *et al.*, 1995; Dreier *et al.*, 1998). We used the $0\ Mg^{2+}$ model of status epilepticus in two *in vitro* preparations; organotypic hippocampal slice cultures and acute slices of temporal cortex. Although organotypic slices were

more excitable than the acute slices, with a greater propensity to generate SLEs and LRD (Supplementary Fig. 2A–D), both preparations generated the well-described transition from SLEs to status epilepticus-like LRD activity (Fig. 2A and Supplementary Fig. 2G). We therefore sought to determine the effect of diazepam on the evolution of *in vitro* seizure-like activity using both these preparations.

First, we showed that diazepam (3 μM) increases the decay time constant (tau) but not the amplitude of voltage-clamp recorded $GABA_AR$ synaptic currents elicited via optogenetic activation of GABAergic interneurons in organotypic brain slices (Supplementary Fig. 1A–F). Furthermore, we then show that diazepam increases both
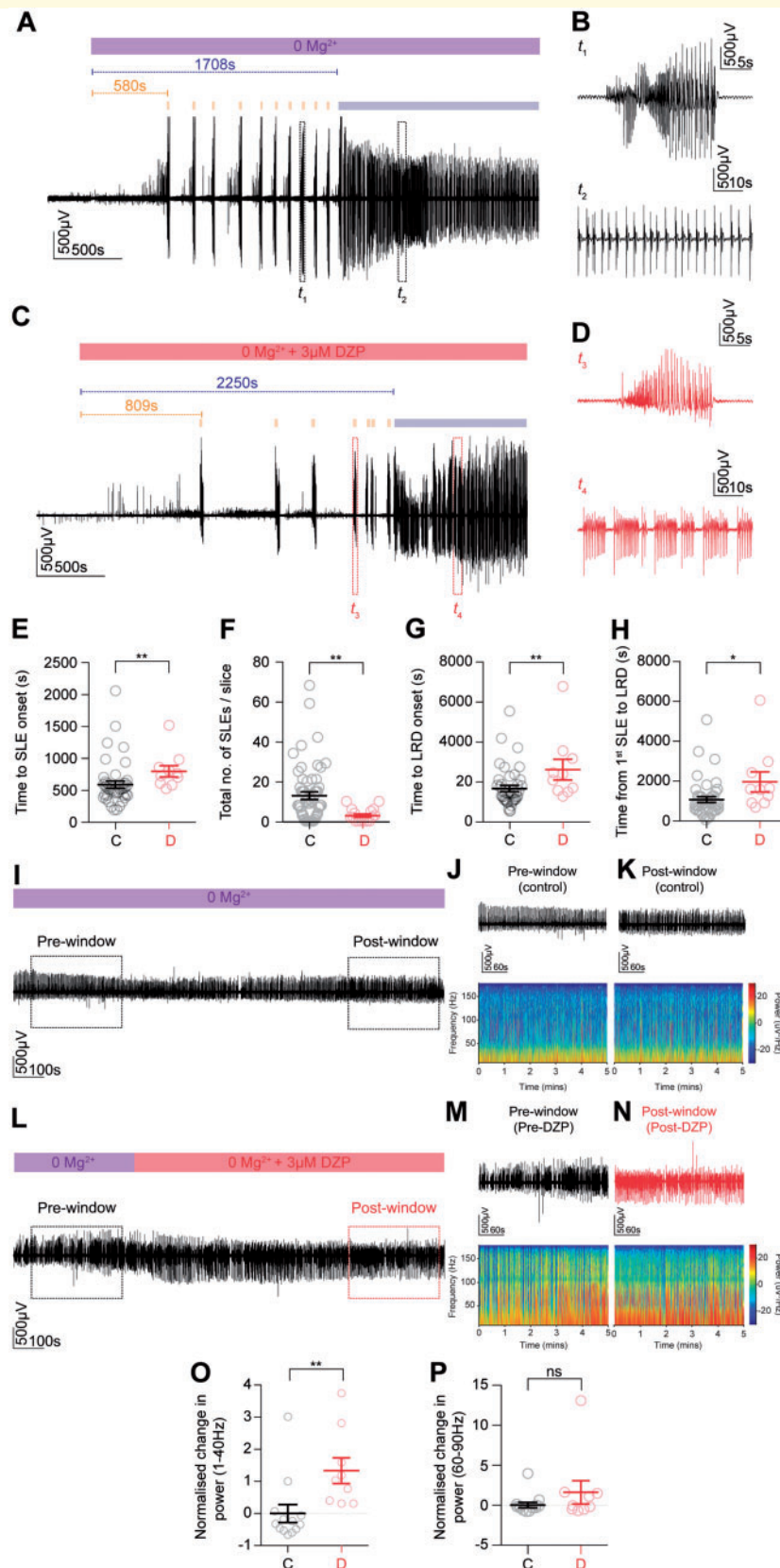
**Figure 2 Early application of diazepam has an antiseizure effect while late application is ineffective and augments epileptiform bursting activity in an *in vitro* model of status epilepticus.** (**A**) The 0 Mg$^{2+}$ chemoconvulsant model was used as an *in vitro* model of status epilepticus (SE) in organotypic hippocampal brain slices. LFP recording from CA1 demonstrating that upon Mg$^{2+}$ withdrawal, activity progressed from single SLEs (orange bars) to a phase where recurrent discharges occurred unabated, the LRD phase (blue bar). (**B**) Window $t_1$ from **A**

(continued)

the amplitude and decay time constant of $GABA_AR$ synaptic currents elicited via electrical stimulation of afferent fibres (3 ms) in acute brain slices in the presence of the glutamate receptor blocker, kynurenic acid (2 μM) Supplementary Fig. 1G–J). In both these preparations the effects of diazepam could be reversed by application of its competitive antagonist, flumazenil (0.4 μM). These findings confirm that GABAergic signalling in both organotypic and acute brain slices is sensitive to diazepam during baseline activity.

We then monitored the evolution of 0 $Mg^{2+}$ induced seizure activity using LFP recordings on interface, while diazepam (3 μM), equivalent to a total clinical dose of 0.75 mg/kg, was either applied 'early', i.e. together with the proconvulsant 0 $Mg^{2+}$ solution (Fig. 2C and Supplementary Fig. 2H), or 'late' once epileptiform activity had already entered the status epilepticus-like LRD phase (Fig. 2L and Supplementary Fig. 2P). Early application of diazepam significantly delayed the onset of SLEs as compared to control slices, which were not exposed to diazepam prior to onset of SLEs (Fig. 2E and Supplementary Fig. 2K). This effect was particularly pronounced in acute slices where early application of diazepam often prevented SLE generation compared to control slices (Supplementary Fig. 2I). Early application of diazepam also caused a significant decline in the total number of SLEs per slice (Fig. 2F and Supplementary Fig. 2L) as compared to control. Moreover, early application of diazepam significantly delayed the onset of LRD in the organotypic brain slices (Fig. 2G) as well as the time between the first SLE and LRD onset (Fig. 2H). The antiseizure effects of diazepam appeared more pronounced in the acute slices where the early diazepam significantly decreased the propensity for SLEs and LRD to (Supplementary Fig. 2I and J). This demonstrated that diazepam had a significant antiseizure effect on the initial pathological discharges in 0 $Mg^{2+}$.

In contrast, we found that in both organotypic and acute brain slices, diazepam lost its antiseizure effect once epileptiform activity had become persistent (status epilepticus-like

activity) and instead enhanced discharges (Fig. 2I–P and Supplementary Fig. 2M–T). To quantify this we measured the power spectral density (PSD) in a 5-min window 1–2 min after the onset of LRD ('pre-window', Fig. 2J, M and Supplementary Fig. 2N and Q) as well as the PSD in a 5-min window 10–15 min following the application of diazepam ('post-window', Fig. 2K, N and Supplementary Fig. 2O and R). In control slices diazepam was not present in the post-window, but this window was taken at an equivalent time period after the pre-window and onset of LRD. This allowed us to calculate the change in power for each slice (post-window power − pre-window power / by pre-window power), which was then normalized by the mean change in power from control slices to generate a metric we term the normalized change in power. We found that in the frequency range 1–40 Hz, diazepam application during LRD significantly increased the normalized change in power as compared to controls in both organotypic (Fig. 2O) and acute (Supplementary Fig. 2S) slices. Diazepam did not significantly affect the normalized change in power in the 60–90 Hz frequency range (Fig. 2P and Supplementary Fig. 2T). Together, this demonstrates that 'late' diazepam application during LRD exacerbates epileptiform activity in two different brain slice preparations.

Phenobarbital, a barbituarate, is also a positive modulator of $GABA_ARs$ and is sometimes used as second-line management for paediatric convulsive status epilepticus refractory to benzodiazepines (Burman *et al.*, 2019). In addition, at higher concentration, it has been shown to antagonize AMPA/kainate receptors (Nardou *et al.*, 2011). We therefore sought to determine the effect of both a low concentration of phenobarbital (100 μM, equivalent to a total clinical dose of 16 mg/kg) and a high concentration of phenobarbital (300 μM, equivalent to a total clinical dose of 49 mg/kg) on late stage status epilepticus-like activity in organotypic brain slices (Supplementary Fig. 3). Strikingly, we found that like diazepam, 100 μM phenobarbital significantly increased the

**Figure 2 Continued**

depicting a single SLE (*top* trace) and window $t_2$ showing recurrent discharges or status epilepticus-like activity (*bottom* trace). (**C**) Early application of diazepam (3 μM) introduced when 0 $Mg^{2+}$ was washed in (red bar). (**D**) Windows $t_1$ and $t_2$ depicting a SLE (*top* trace) and status epilepticus-like activity (*bottom* trace) in diazepam. (**E**) Population data showing that early diazepam application delays the onset of SLEs (control, n = 41: median 510.0, IQR 412.6–616.2 s versus diazepam, n = 10: median 736.3, IQR 594.4–883.0 s, P = 0.003, Mann-Whitney U-test) while decreasing the total number of SLEs (**F**, control: median 9.0, IQR 2.3–19.3 versus diazepam: median 2.0 IQR 0.0–5.8, P = 0.001, Mann-Whitney U-test), retarding onset of LRD (**G**, control: median 1386, IQR 1087–1966 s versus diazepam: 2220 IQR 1522–3236 s, P = 0.01, Mann-Whitney U-test) and extending the time from first SLE to LRD (**H**, control: median 799.8, IQR 501.4–1228 s versus diazepam: median 1555 s, IQR 874.2–2529 s, P = 0.01, Mann-Whitney U-test). (**I**) LFP recording of the LRD phase in a control slice, with a 5 min pre- and post-window used for analysis (dashed rectangles). (**J**) Pre-window LFP trace (*top*) with its associated spectrogram (*bottom*). (**K**) Post-window as in **J**. (**L**) LFP recording of LRD with diazepam application and accompanying pre-window (**M**) and post-window (**N**) (dashed rectangles) used for analysis. (**O**) Population data demonstrating raised normalized change in power of status epilepticus-like activity in the 1–40 Hz frequency range between diazepam and control slices (control, n = 13: median −0.3, IQR −0.5 to −0.01 versus diazepam, n = 9: median 1.0, IQR 0.3–2.2, P = 0.001, Mann-Whitney U-test). (**P**) No statistical difference in normalized change in power between groups was observed in the 60–90 Hz range (control: median −0.3, IQR −0.6 to −0.02 versus diazepam: median −0.18, IQR −0.6–1.5, P = 0.4, Mann-Whitney U-test). DZP = diazepam. $^*P \leqslant 0.05$; $^{**}P \leqslant 0.01$; ns = not significant ($P \geqslant 0.05$); error bars indicate mean ± SEM.

normalized change in power (1–40 Hz) compared to controls (Supplementary Fig. 3A–C and G). In contrast, 300 μM phenobarbital attenuated status epilepticus-like activity, significantly reducing the normalized change in power (1–40 Hz) compared to controls (Supplementary Fig. 3D–F and G). No significant changes were observed in the 60–90 Hz frequency range.

## Persistent epileptiform activity is associated with a reduction in GABAergic synaptic conductances

Having observed that diazepam and low dose phenobarbital lost their antiseizure efficacy during LRD, we next sought to determine whether synaptic $GABA_A R$ internalization (Goodkin et al., 2005) and hence a reduction in GABA synaptic conductance ($g_{GABA}$) could underlie this effect.

We optogenetically activated GABAergic neurons, and recorded postsynaptic GABA-R mediated currents, in voltage-clamp mode, in CA1 pyramidal neurons in mouse organotypic slice cultures (Fig. 3A). By recording GABA currents at different holding voltages $g_{GABA}$ could be measured before and after 30 min exposure to 0 $Mg^{2+}$ and confirmation of LRD in the same neuron. $GABA_B$ receptor blockade to isolate $GABA_A Rs$ was not used as this could interfere with the seizure-like activity evoked by 0 $Mg^{2+}$ (Swartzwelder et al., 1987; Codadu et al., 2019). Following termination of status epilepticus-like activity using reintroduction of $Mg^{2+}$, $g_{GABA}$ was remeasured. The mean $g_{GABA}$ elicited under baseline conditions decreased after status epilepticus-like activity had been arrested (Fig. 3B–D), with no significant change in access resistance (baseline: mean 15.68 ± SEM 1.03 MΩ

versus 30 min after 0 $Mg^{2+}$: mean 18.60 ± SEM 1.18 MΩ, $P$ = 0.11, paired $t$-test, data not shown). These findings demonstrate that status epilepticus-like activity is associated with reductions in GABA synaptic conductances, which is most likely caused by $GABA_A R$ internalization (Goodkin et al., 2005). Nonetheless, despite prolonged periods of persistent seizure-like activity in vitro, optogenetic activation of GABAergic interneurons could still reliably evoke GABA synaptic currents.

## Status epilepticus-like activity is accompanied by compromised neuronal $Cl^-$ extrusion

We surmised that additional mechanisms to $GABA_A R$ internalization must also play a role in the loss of diazepam's antiseizure efficacy during LRD. This is because $GABA_A R$ internalization cannot explain how diazepam and low dose phenobarbital could exacerbate epileptiform discharges during status epilepticus-like activity. Intracellular $Cl^-$ accumulation and a depolarizing shift in $E_{GABA}$, could potentially explain this phenomenon. To explore whether status epilepticus-like activity might compromise $Cl^-$ extrusion mechanisms in neurons we performed gramicidin perforated patch-clamp recordings from hippocampal pyramidal cells. This technique avoids disrupting the $[Cl^-]_i$ of the neuron. Somatic application of GABA agonists (GABA, or muscimol) was used to record $E_{GABA}$ under quiescent network conditions to assess steady state changes in $Cl^-$ extrusion (Fig. 4A). $E_{GABA}$ was measured using voltage step protocols, before $Mg^{2+}$ removal (baseline) and after different periods of induced status epilepticus-like activity had
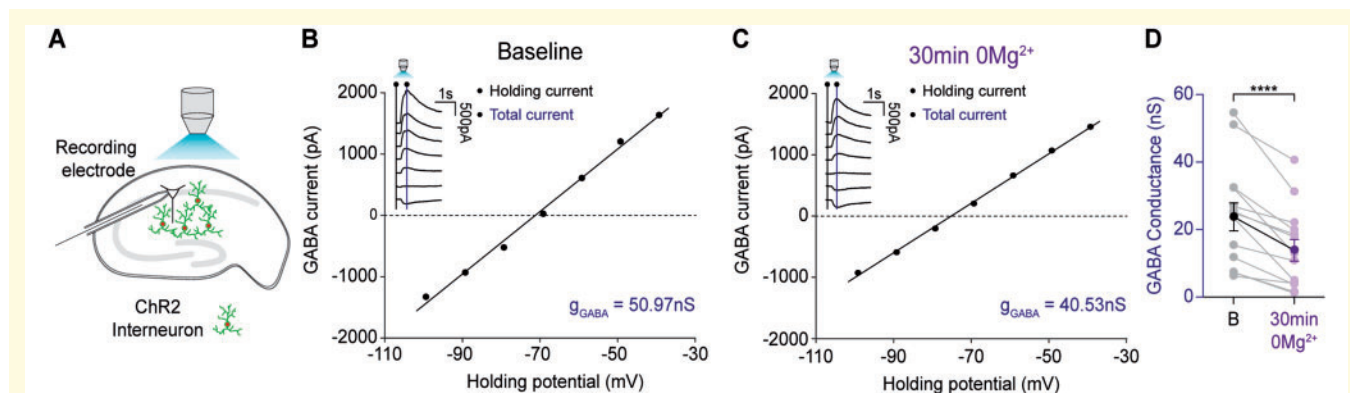


**Figure 3 Persistent epileptiform activity is associated with a reduction in GABAergic synaptic conductance.** (**A**) Schematic of experimental setup showing whole-cell recordings being performed from CA1 pyramidal neurons in mouse organotypic brain slices where GAD2+ interneurons were transfected with ChR2-YFP and activated using a high-powered LED coupled to the objective. (**B**) Example GABA I-V plot from a whole-cell patch-clamp recording (low $Cl^-$ internal, 10 mM) of a CA1 pyramidal cell in a mouse hippocampal organotypic slice. Inset: Raw current traces recorded at different holding potentials. GABA was evoked by optogenetic activation of ChR2 expressing GAD2+ interneurons with 100 ms blue light pulses. GABA conductance ($g_{GABA}$) was calculated from the slope of the GABA current I-V curve. The GABA current was calculated by subtracting the holding current (black line on inset) from the total current (blue line on inset) for each holding potential. (**C**) Example GABA I-V plot from the same cell as in **B** following cessation of persistent epileptiform activity generated by 30 min of 0 $Mg^{2+}$ application. (**D**) Population data ($n$ = 14) showing a significant decrease in $g_{GABA}$ from baseline to after 30 min 0 $Mg^{2+}$ (baseline: mean 23.6 ± SEM 4.1 nS versus 30 min of 0 $Mg^{2+}$: mean 13.1 ± SEM 3.2 nS, $P$ = 0.0001, paired $t$-test). ****$P \leqslant$ 0.0001; error bars indicate mean ± SEM.
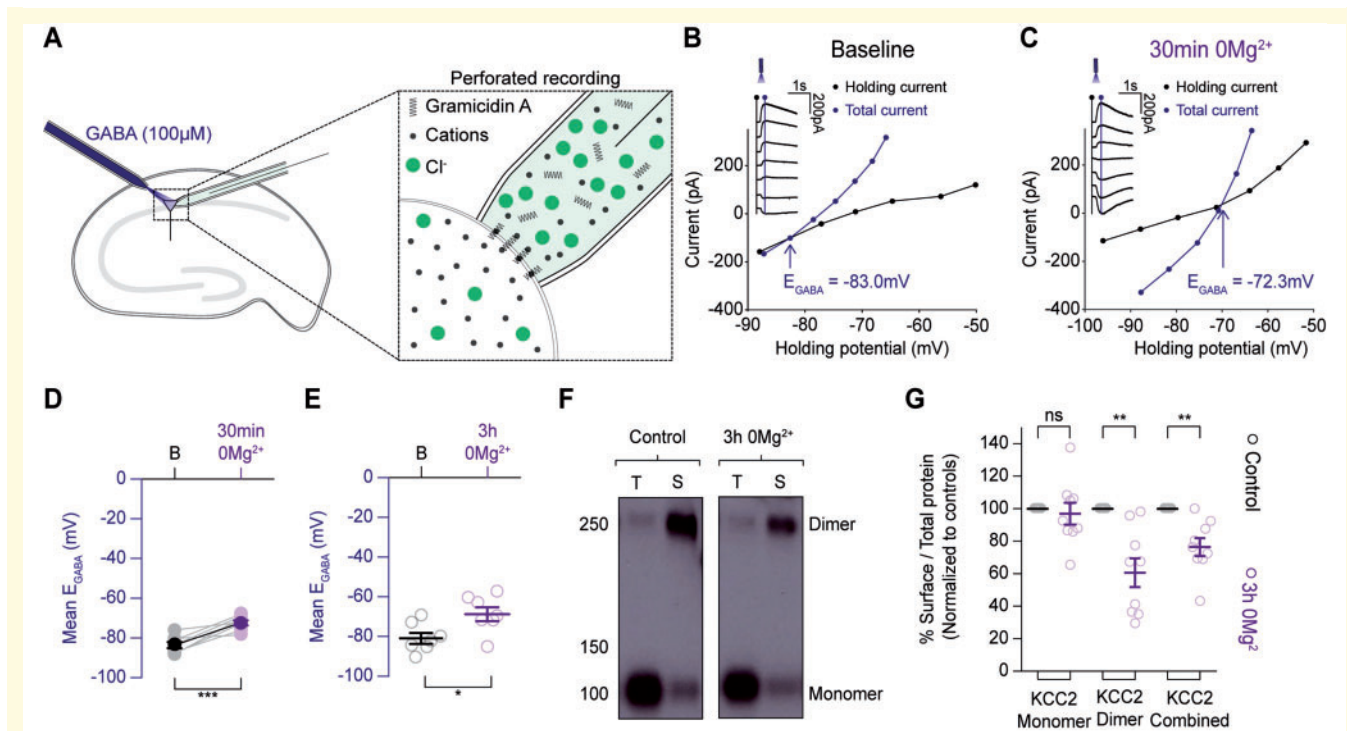
**Figure 4 Status epilepticus-like activity is associated with compromised neuronal Cl⁻ extrusion.** (**A**) Schematic demonstrating the gramicidin perforated patch-clamp recording configuration from organotypic hippocampal pyramidal cells and accompanying somatic GABA application. (**B**) Example recording from a mouse CA1 pyramidal neuron. Resting $E_{GABA}$ was measured by delivering GABA puffs at different holding potentials (inset). I–V curves were then plotted featuring the holding current (reflecting membrane current, black) and total current (reflecting membrane current plus the GABA-evoked current, blue). $E_{GABA}$ was calculated as the potential at which the total current (blue line) was equal to the holding current (black line). (**C**) Following 30 min of $Mg^{2+}$ withdrawal, epileptiform activity was arrested by reintroducing $Mg^{2+}$ into the artificial CSF and resting $E_{GABA}$ was once again measured as in **B**. (**D**) Population data ($n = 8$) showing a significant increase in $E_{GABA}$ between baseline and after a period of persistent seizure-like activity induced by 30 min of 0 $Mg^{2+}$ application (resting: mean $-83.4 \pm$ SEM 1.5 mV versus after 30 min 0 $Mg^{2+}$: mean $-72.3 \pm$ SEM 1.2 mV, $P = 0.0008$, paired $t$-test). (**E**) Population data ($n = 7$) from a similar experiment as in **F** from rat organotypic brain slices cultures and 3 h of $Mg^{2+}$ withdrawal demonstrating a further increase in $E_{GABA}$ following this extended period of persistent epileptiform activity (resting: mean $-80.8 \pm$ SEM 2.8 mV versus after 3 h 0 $Mg^{2+}$: $-68.6 \pm$ SEM 3.5 mV, $P = 0.02$, unpaired $t$-test). (**F**) Western blots of control hippocampal slices, and those that had been treated with 3 h of 0 $Mg^{2+}$. Cell homogenates ('T'-total) and NeutrAvidin captured cell surface proteins ('S'-surface) were probed on western blots with the anti-C-terminus KCC2 antibody. 0 $Mg^{2+}$ blots showed weaker bands for surface-bound KCC2 dimers, but little change in monomers compared to controls. (**G**) Surface proteins from hippocampal slice lysates were quantified by the ratio of surface to total optical density. Values were then normalized to a percentage of untreated control values. Three hours of 0 $Mg^{2+}$ treatment significantly reduced the surface: total ratio of overall KCC2 as compared to controls (surface KCC2 reduction, $n = 9$: 76.4 $\pm$ SEM 0.05% of control, $P = 0.003$, unpaired $t$-test). This change reflected a specific reduction in the surface levels of KCC2 dimers (surface KCC2 dimer reduction: 60.6 $\pm$ SEM 8.8% of control, $P = 0.002$, unpaired $t$-test). In contrast, monomeric KCC2 showed little difference across the two conditions with the mean in the 0 $Mg^{2+}$ condition at (reduction of KCC2 monomer: 97.0 $\pm$ SEM 6.7% of control, $P = 0.66$, unpaired $t$-test) *$P \leqslant 0.05$; **$P \leqslant 0.01$; ns = not significant ($P \geqslant 0.05$).

been arrested by reintroducing $Mg^{2+}$. We found that in the hippocampal organotypic brain slices, resting $E_{GABA}$ became more depolarized after a period of 30 min of $Mg^{2+}$ withdrawal (Fig. 4B–D). We investigated this effect further in rat hippocampal organotypic slices, extending the period of 0 $Mg^{2+}$ withdrawal and putative status epilepticus-like activity to 3 h. This also resulted in $E_{GABA}$ becoming more depolarized (Fig. 4E).

We next used surface biotinylation and western blotting for the major cation-chloride cotransporter (KCC2) to determine whether the depolarizing shift in $E_{GABA}$ was accompanied by a shift in the cell surface expression of KCC2. Indeed, on average, the total amount of surface KCC2 in organotypic hippocampal slices treated with 0 $Mg^{2+}$ was reduced to mean 76.4 $\pm$ SEM 0.05% of that found in control slices (Fig. 4F and G). When KCC2 was further subdivided into monomeric and dimeric forms it was found that this drop-in surface protein was almost exclusively due to a reduction in the KCC2 dimer. Zero $Mg^{2+}$ treatment reduced the levels of surface bound KCC2 dimer significantly compared to controls. These findings confirm previous reports (Rivera *et al.*, 2004) that prolonged seizure activity results in a reduction in expression of KCC2 and a depolarizing shift in steady-state $E_{GABA}$.

## Persistent epileptiform activity drives pronounced depolarizing shifts in $E_{GABA}$ and intracellular $Cl^-$ accumulation

The shifts in steady-state $E_{GABA}$ we observed above are unlikely to explain the enhancing effect of diazepam on burst discharges we observed during status epilepticus-like activity. This is because resting $E_{GABA}$'s of $\sim-60$ mV are typically below the action potential threshold from of CA1 neurons in our preparation (action potential threshold: mean $-38.72 \pm$ SEM 5.45 mV, $n = 17$, data not shown) and thus would still render $GABA_AR$-mediated transmission inhibitory. We therefore surmised that compromised $Cl^-$ extrusion combined with the activity-dependent $Cl^-$ loading during status epilepticus-like activity could result in more severe shifts in $E_{GABA}$.

To explore this possibility, we modified our gramicidin perforated patch-clamp recording protocols to track dynamic changes in $E_{GABA}$ during the evolution of epileptiform activity in the 0 $Mg^{2+}$ model (Fig. 5A). The recording configuration was rapidly switched between current-clamp mode to measure membrane potential and short periods in voltage-clamp mode, during which a voltage ramp protocol and somatic GABA puff was applied, to provide a rapid estimate of $E_{GABA}$ (Fig. 5B). Compared to baseline, SLEs and status epilepticus-like activity (LRD phase) were associated with pronounced increases in $E_{GABA}$ (Fig. 5C and D). Once persistent epileptiform activity was terminated by TTX, $E_{GABA}$ decreased but did not return to baseline levels. The $E_{GABA}$ remained moderately but persistently depolarized, further confirming the long-term shifts in $Cl^-$ extrusion mechanisms described above. These experiments demonstrated $E_{GABA}$ to be highly dynamic. Status epilepticus-like activity was associated with profound elevations in $E_{GABA}$ to values comparable to the action potential threshold for these neurons, which would render $GABA_AR$ mediated transmission excitatory.

To measure changes in $Cl^-$ concentration directly, which could underlie the observed activity driven shifts in $E_{GABA}$, we used the genetically-encoded reporter of $Cl^-$, ClopHensorN. This reporter enables pH-corrected estimates of intracellular $Cl^-$ concentration (Arosio *et al.*, 2010; Raimondo *et al.*, 2013; Sato *et al.*, 2017). Biolistic transfection of mouse organotypic hippocampal brain slices resulted in sparse ClopHensorN expression within pyramidal neurons. Confocal imaging of ClopHensorN expressing cells was performed concurrently with whole cell patch-clamp recordings of neighbouring cells to provide a simultaneous readout of seizure-like activity (Fig. 5C–E). SLEs and the LRD phase were associated with increases in $[Cl^-]_i$ (Fig. 5E and F). Importantly, the LRD phase was associated with a significant increase in $[Cl^-]_i$. These results suggest that *in vitro* status epilepticus-like activity is accompanied by profound short-term, activity-driven increases in $E_{GABA}$ and $[Cl^-]_i$.

To determine whether the canonically inward $Cl^-$ cotransporter (NKCC1), might contribute to $Cl^-$ accumulation and the effects of diazepam on late stage status epilepticus-like activity, we repeated the interface experiments in Fig. 2I–Q, but combined diazepam application with 10 µM bumetanide to block NKCC1 activity (Supplementary Fig. 4). We found that the addition of bumetanide did not significantly alter the normalized change in power as compared to control slices or to diazepam application alone (Supplementary Fig. 4A–E). This result suggests that blocking NKCC1 during LRD does not rescue the antiseizure effects of diazepam during this phase of epileptiform activity.

## GABA-releasing interneurons are active and highly correlated with pyramidal cell activity during the LRD phase

Having observed significant increases in $E_{GABA}$ and intracellular $Cl^-$ in pyramidal neurons during the LRD phase of the 0 $Mg^{2+}$ model of status epilepticus, we next aimed to determine how the activity of GABA-releasing interneurons might relate to that of pyramidal cells during the recurrent discharges observed in this period. To this end we used organotypic slices prepared from mice where the cre-lox system was used to selectively express the red fluorescent reporter tdTomato under the glutamic acid decarboxylase type 2 (*GAD2*) promoter. Using dual whole-cell patch-clamp, we made targeted recordings from CA1 hippocampal GABAergic interneurons and pyramidal cells during various phases of seizure-like activity in the 0 $Mg^{2+}$ *in vitro* model of status epilepticus (Fig. 6A). We noticed that GABAergic interneurons were highly active during the LRD phase (Fig. 6C and D). To determine whether the activity of GABAergic interneurons was synchronized with that of pyramidal cells we used linear correlation as a measure of synchrony (Jiruska *et al.*, 2013). We compared the synchrony during baseline, single SLEs, during the LRD phase and following cessation of epileptiform activity (post-LRD). The correlation and hence synchrony between interneurons and pyramidal cells was increased during SLEs and LRD as compared to pre- and post-epileptiform activity (Fig. 6D and E). Synchrony between these two cell types was significantly higher during LRD as compared to SLEs, which demonstrates that persistent epileptiform activity is composed of highly synchronous activity between GABAergic interneurons and glutamatergic pyramidal cells.

## GABAergic signalling is strongly depolarizing during the late recurrent discharge phase

Given our observations of a depolarizing $E_{GABA}$ and highly synchronized GABAergic interneuronal and pyramidal cell
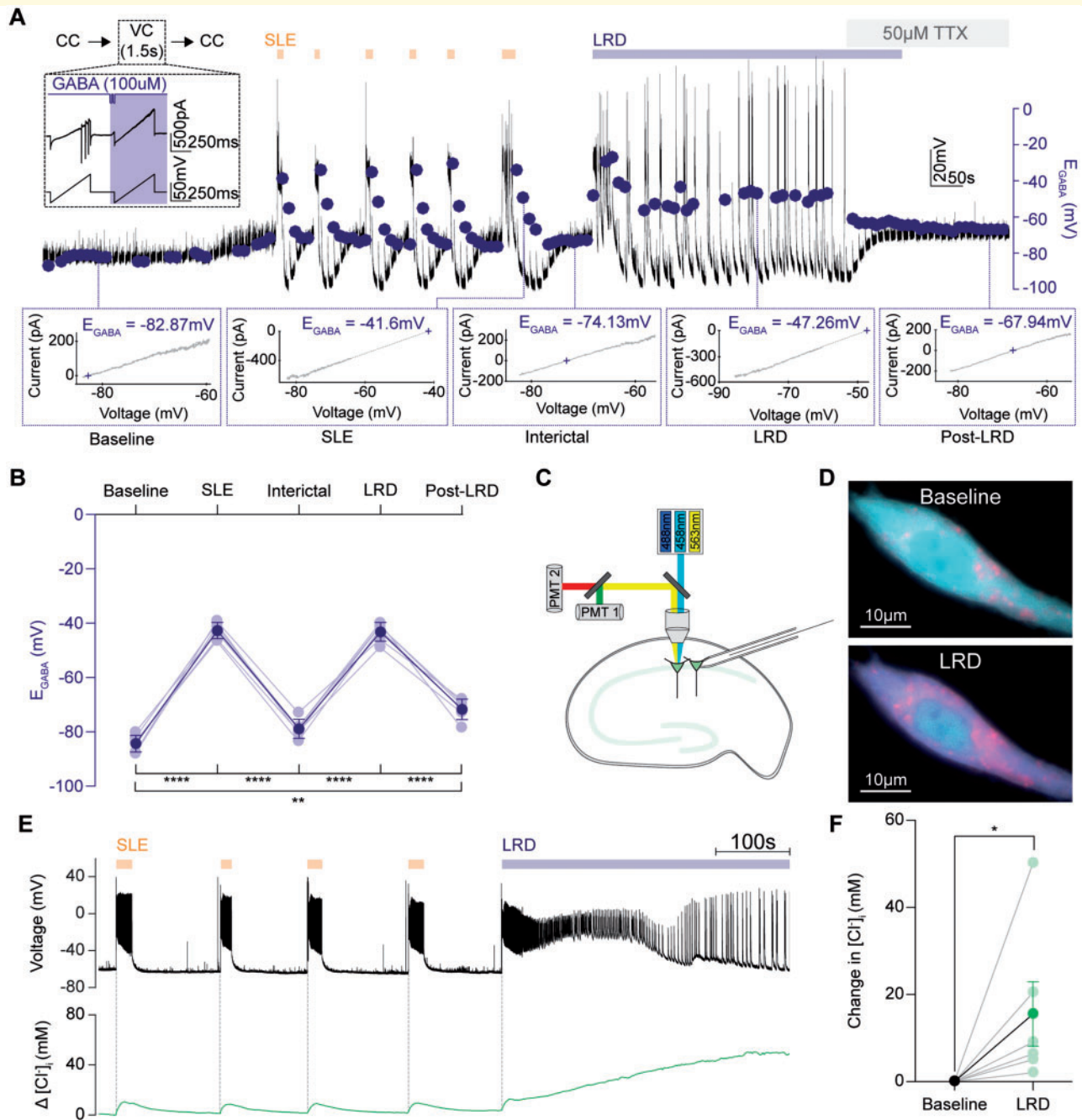
**Figure 5 Persistent seizure-like activity drives pronounced depolarizing shifts in $E_{GABA}$ and intracellular $Cl^-$ accumulation.**
(**A**) To measure $E_{GABA}$ during epileptiform activity, gramicidin perforated patch-clamp recordings were performed and the recording mode was rapidly switched from current-clamp (CC) to brief periods in voltage clamp (1.5-s duration) every 10 s (inset). While in voltage-clamp, two consecutive voltage ramps were applied: the first without GABA application; and the second paired with GABA application (blue) applied to the soma. A representative recording from a CA1 pyramidal neuron where $E_{GABA}$ measurements (blue dots) were made throughout the progression of epileptiform activity in the 0 $Mg^{2+}$ model (orange arrows shows SLEs, blue bar depicts LRD). Dotted lines highlight periods during evolution of epileptiform activity: baseline ($t_1$), immediately following SLEs ($t_2$), between SLEs / interictal ($t_3$), LRD ($t_4$), following termination of activity / post-LRD ($t_5$). To rapidly abort epileptiform activity during LRD, TTX (50 μM) was applied. *Bottom*: I-V plots were used to calculate $E_{GABA}$ defined as the voltage at which the GABA current equals 0 ($t_{1-5}$). (**B**) Population data showing significant changes in $E_{GABA}$ between the different periods. $E_{GABA}$ shifted from mean baseline levels of mean $-83.9 \pm$ SEM 1.1 mV to mean $-42.7 \pm$ SEM 1.0 mV during SLEs ($n = 7$, $P < 0.0001$, paired $t$-test) before partially recovering to a mean level of mean $-78.9 \pm$ SEM 1.1 mV between events ($P < 0.0001$, paired $t$-test). Status epilepticus-like activity (LRD phase) profoundly elevated $E_{GABA}$ again to mean $-43.2 \pm$ SEM 1.9 mV ($P < 0.0001$ as compared to baseline, paired $t$-test). $E_{GABA}$ levels were equally high during SLEs and the LRD phase (SLE: mean $-42.7 \pm$ SEM 1.04 mV versus LRD: mean $-43.2 \pm$ SEM 1.9 mV, $P = 0.73$, paired $t$-test). Following termination of the LRD phase with TTX, the EGABA decreased but remained more depolarized compared to the baseline $E_{GABA}$ (baseline: mean $-83.9 \pm$ SEM 1.13 mV versus recovery: mean

(continued)

activity during the status epilepticus-like activity of the LRD phase, we next explored whether GABAergic signalling might in fact be excitatory during LRD. To investigate this, we used an optogenetic approach to isolate and selectively activate ChR2-expressing GABAergic (GAD2+) interneurons during different phases of seizure-like activity. Using this experimental setup, GABAergic interneurons were activated every 7 s with 100 ms of blue light while performing whole-cell current-clamp recordings from CA1 pyramidal neurons during the progression of seizure-like activity in the 0 $Mg^{2+}$ model.

We observed that while light activation resulted in hyperpolarizing synaptic potentials under baseline conditions, (Fig. 7A–C), during single SLEs, light delivery reliably triggered membrane depolarization and the generation of action potentials (Fig. 7B and C). Inbetween SLEs, the hyperpolarizing responses to optogenetic activation were restored. However, during the status epilepticus-like LRD phase, light activation again consistently resulted in strong depolarization and action potentials in the recorded neurons (Fig. 7C).

We then repeated this with cells held at −40 mV in the voltage-clamp configuration to record light-induced synaptic currents (Fig. 7D–F). After SLEs had self-terminated, light-induced currents returned to positive values. During the LRD phase, the currents recorded in pyramidal neurons following optogenetic activation of GABAergic interneurons again became significantly negative. This could be reversed when persistent epileptiform activity was terminated using reintroduction of $Mg^{2+}$-containing artificial CSF. Taken together, these data demonstrated that GABAergic interneurons have profound excitatory effects on their synaptic targets during persistent epileptiform activity in the 0 $Mg^{2+}$ model.

## Interneurons trigger epileptiform discharges and entrain the network during persistent epileptiform activity

Our data suggest that the GABAergic inhibitory system becomes ineffective during status epilepticus-like activity due to changes in chloride homeostasis and this could explain the failure of diazepam to reduce seizure-like activity during this phase. To test this hypothesis further, we next sought to determine whether recruitment of GABAergic interneurons fails to inhibit epileptiform activity during LRD and furthermore, whether selective activation of interneurons results in more pro-seizure like effects than anti-seizure activity as was witnessed following diazepam application in our preparation.

During a 5-min analysis period during the LRD phase, we analysed our traces in 7-s windows to determine what effect selective activation of GABAergic interneurons (100 ms blue light activation occurring 3.5 s into the 7-s window) had on epileptiform activity. This 7-s window was then divided into smaller 200-ms time bins whereby the probability of an epileptiform discharge being initiated could be calculated (Fig. 8A–D). Discharges were defined as inward currents >10 SD from baseline noise and lasting more than 500 ms. We observed that the probability of discharge initiation increased to mean 0.78 ± SEM 0.06 during the 200 ms immediately following light application. In a control experiment repetitive light activation was initiated only after a minimum of 5 min of LRD activity had occurred. The probability of discharge initiation within the 200-ms time bin 3.5 s into the 7-s window increased when the light was delivered at the start of this time bin (Fig. 8E–I).

Having established that optogenetic activation of GABAergic interneurons reliably initiated epileptiform discharges during status epilepticus-like activity, we next sought to determine whether excitatory $GABA_AR$ synaptic signalling was responsible for this effect. To this end we added the $GABA_AR$ antagonist picrotoxin (100 μM) to the perfusing artificial CSF after at least 5 min of LRD activity had been induced (Fig. 8J–N). The picrotoxin did not arrest the LRD activity demonstrating that $GABA_AR$-mediated synaptic transmission is not necessary for the generation of these discharges. However, we did note that the probability of discharge initiation following optogenetic activation of GABAergic interneurons decreased significantly (Fig. 8J–N). This confirmed that $GABA_AR$ mediated transmission is necessary for the pro-seizure properties of the GABAergic interneuronal network during LRD.
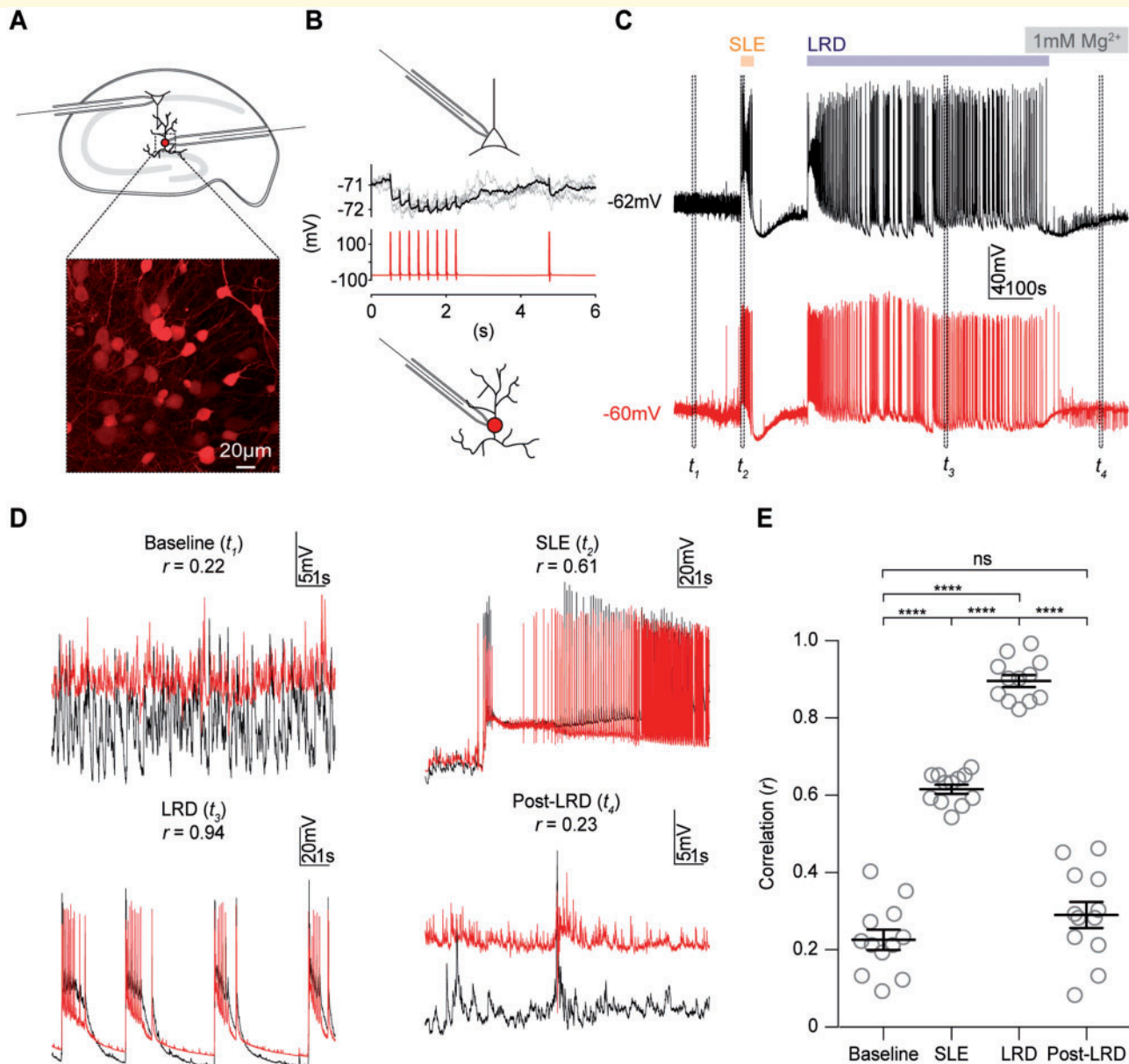
**Figure 6 GABA-releasing interneurons are active and highly correlated with pyramidal cell activity during the late recurrent discharge phase.** (**A**) Diagram of the experimental setup (*top*), which involved simultaneous whole-cell patch-clamp recordings from CA1 pyramidal neurons and GABAergic interneurons in organotypic hippocampal brain slices (*n* = 12). Inset: Confocal images show interneurons in the stratum radiatum expressing tdTomato using the cre-lox system (tdTomato reporter line crossed with GAD2-cre line). (**B**) GABAergic connection between pyramidal cell (black) and GAD2+ interneuron (red) confirmed by observing negative shifts in the pyramidal cell membrane potential when action potentials were generated in the interneuron. Only 3 of 12 paired recordings showed functional inhibitory synaptic connections. (**C**) Dual current-clamp recordings from the same cells in **B** during progression of 0 $Mg^{2+}$ seizure-like activity. Four periods are denoted by dashed rectangles: baseline ($t_1$), at the start of a single SLE ($t_2$), during the LRD phase ($t_3$) and after epileptiform activity had been aborted with the re-introduction of 1 mM $Mg^{2+}$, post-LRD ($t_4$). (**D**) Insets show the four periods in **C**, with recordings from the two neurons superimposed to reveal the extent of synchronous activity. The Pearson's coefficient (*r*) was calculated from a direct linear correlation of the two raw traces during each epoch (8-s duration). (**E**) Population data showing significant increases in correlation during single SLEs ($t_2$) and the LRD phase ($t_4$) (baseline mean *r* = 0.2 ± SEM 0.03; SLEs mean *r* = 0.6 ± SEM 0.01; LRD mean *r* = 0.90 ± SEM 0.02, post mean *r* = 0.29 ± SEM 0.03, *P* < 0.0001, paired *t*-tests,). Furthermore, the synchrony between pyramidal cells and interneurons was greater during LRD compared to during single SLEs (mean *r* = 0.9 versus mean *r* = 0.6, *P* < 0.0001, paired *t*-test). GAD2 = glutamic acid decarboxylase 2; ns = non-significant; SR = stratum radiatum; Td = tandem dimeric tomato. ****$P \leqslant 0.0001$; ns = not significant ($P \geqslant 0.05$); error bars indicate mean ± SEM.
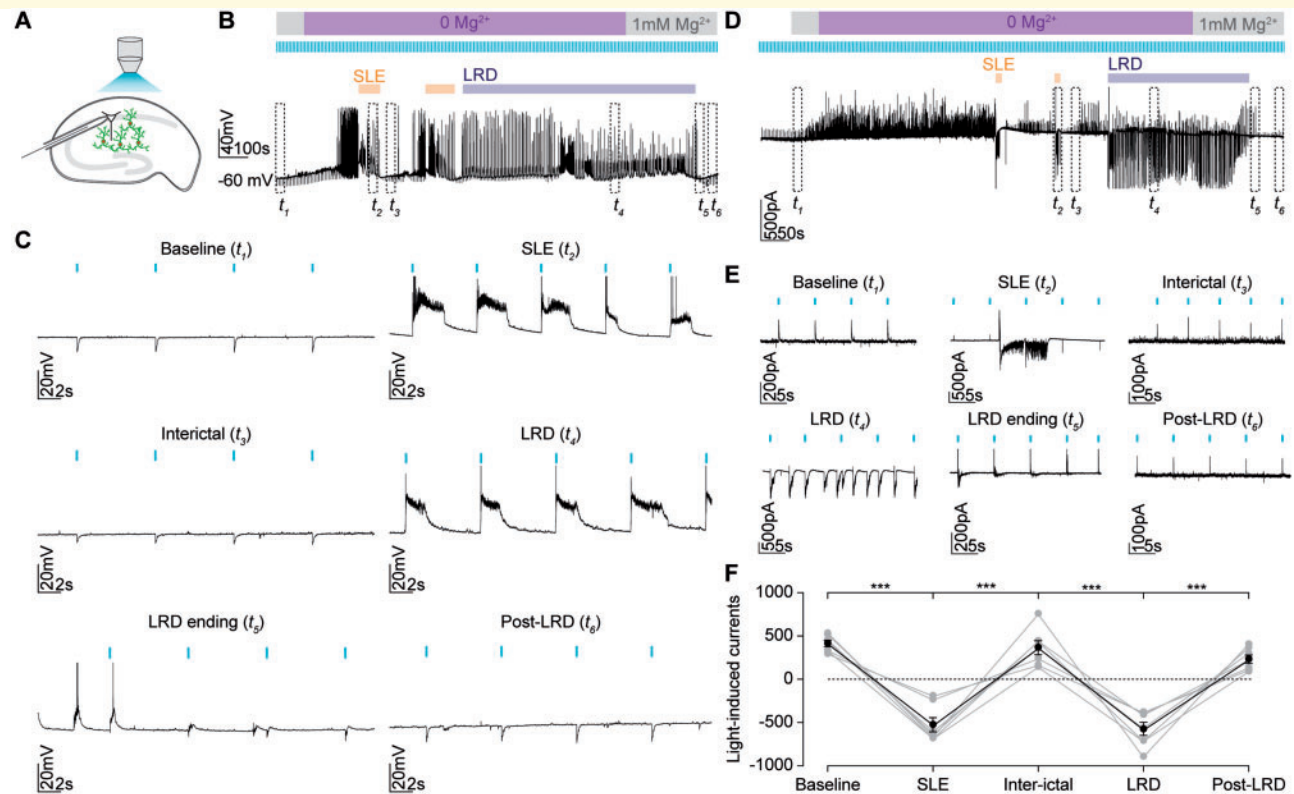
**Figure 7 GABAergic signalling is strongly depolarizing during the late recurrent discharge phase.** (**A**) Experimental setup showing whole-cell recordings being performed from CA1 pyramidal neurons in mouse organotypic brain slices where GAD2+ interneurons were transfected with ChR2-YFP and activated using a high-powered LED coupled to the objective. (**B**) Current-clamp recording with optogenetic activation of GAD2+ interneurons every 7 s using 100 ms light pulses during the evolution of epileptiform activity in $Mg^{2+}$-free solution. Individual SLEs (orange bars) and LRD are indicated (blue bar). The persistent activity of the LRD phase was terminated using artificial CSF containing 1mM $Mg^{2+}$. The dashed rectangles $t_{1-6}$ represent 30-s windows from different periods: baseline ($t_1$), latter portion of a SLE ($t_2$), interictal period ($t_3$), LRD ($t_4$), LRD ending ($t_5$) and post-LRD ($t_6$). (**C**) Expanded view of the windows $t_{1-6}$ in **B** show optogenetic activation of GAD2+ interneurons (blue bars) shifting from causing membrane hyperpolarization during baseline and interictal periods to membrane depolarization and action potentials during SLEs and LRD. These effects were transient with the cessation of LRD resulting in a return of inhibitory postsynaptic potentials. (**D**) Voltage-clamp recording from CA1 pyramidal cell clamped at −40 mV to record light-induced currents using the protocol as in **B**. Dashed rectangles representing the same periods as in **B**. (**E**) Expanded views of $t_{1-6}$ showing changes in the maximum light-induced currents at each phase of activity. (**F**) Population data ($n = 7$) showing significant changes in current size and direction across the different phases. Light currents were recorded as the maximum light induced current within 100 ms of the light pulse. At rest these were outward (positive), with a mean value of mean 448.8 ± SEM 70.3 pA but rapidly flipped to being inward (negative) during SLEs (mean −752 ± SEM 88.7 pA, $P = 0.0002$, paired $t$-test). After the SLE had recovered, the currents returned to positive values (mean 536.5 ± SEM 134.9 pA, $P = 0.0007$). However, during the LRD phase the currents again became significantly negative compared to the preceding interictal period (mean −894.0 ± SEM 164.8 pA, $P = 0.0018$, paired $t$-test). When Mg was re-introduced, the current again shifted to become positive (mean 242.0 ± SEM 21.2 pA, $P = 0.0005$, paired $t$-test). There was no significant difference in amplitude between light-induced currents during SLE and LRD (SLE: mean −752.00 ± SEM 88.67 pA versus LRD: mean −894.00 ± SEM 164.80 pA, $P = 0.18$, paired $t$-test). ***$P \leqslant 0.001$; error bars indicate mean ± SEM.

Finally, we measured changes in the frequency of epileptiform discharges during LRD when GABAergic interneurons were optogenetically activated at 0.14 Hz ('on'), when the light was not applied ('off') and when optogenetic activation occurred in the presence of 100 μM picrotoxin. As demonstrated in Fig. 8O and P, in the on condition, the frequency of discharges was entrained either to the frequency of light delivery (0.14 Hz) or twice the frequency (0.28 Hz), indicating one 'break through' discharge every cycle. By comparison, if there was no light activation or picrotoxin was present, there was a wide distribution of discharge frequencies. In addition, there was a significantly smaller difference between the frequency at which the light was delivered and the frequency of discharges between the on group as compared to the off, and picrotoxin groups (Fig. 8Q). Taken together these data demonstrate that GABAergic interneurons are ineffective at curtailing epileptiform discharges during status epilepticus-like activity and can enhance epileptiform activity.
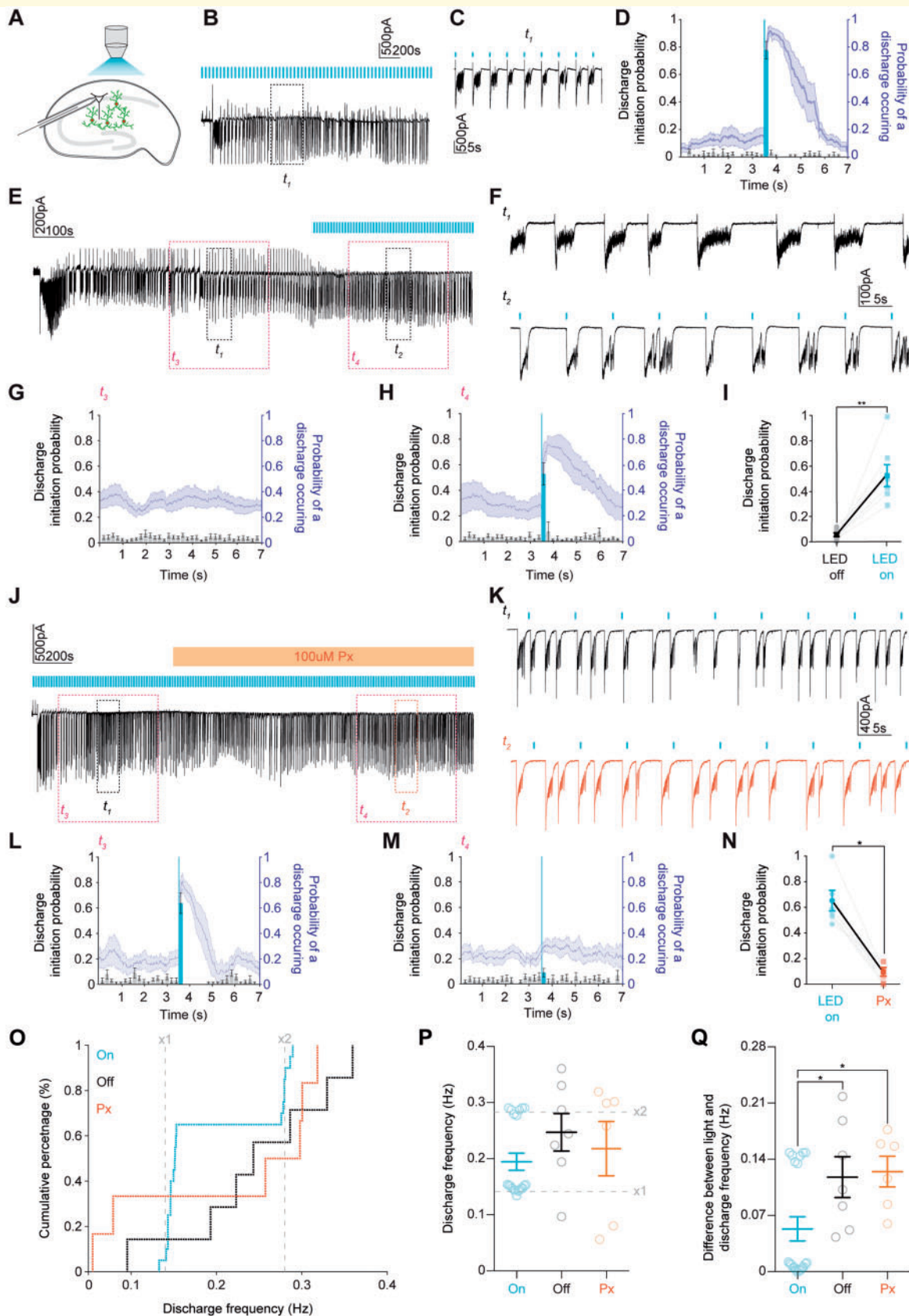
**Figure 8 Optogenetic activation of GABAergic interneurons during LRD triggers burst discharges and entrains the hippo-campal network in a GABA$_A$R dependent manner.** (**A**) Experimental schematic showing whole-cell patch-clamp recordings from CA1 pyramidal neurons with widefield optogenetic activation of GAD2+ interneurons. (**B**) Voltage-clamp recording during LRD from a cell clamped at

# Discussion

In our study we used clinical and experimental data to explore the phenomenon of benzodiazepine-resistant status epilepticus. We found that the prevalence of benzodiazepine resistance in a South African cohort of paediatric patients in status epilepticus is similar to that observed internationally (Chin *et al.*, 2008). In addition, our clinical data confirm several prior observations that provide some critical insights into the underlying pathology and clinical management. First, benzodiazepine-resistant status epilepticus is associated with increased morbidity in patients (Chin *et al.*, 2008). Second, patients who seize for longer prior to initial treatment were more likely to be resistant to benzodiazepine treatment. While previous studies and reviews have alluded to longer status epilepticus duration being associated with increased resistance to benzodiazepines (Deeb *et al.*, 2012; Naylor, 2014; Fernández *et al.*, 2015; Gaínza-Lein *et al.*, 2018, 2019), our clinical data are the first to quantify this phenomenon. Notably, we show that the duration of status epilepticus can successfully be used as a binary classifier to detect benzodiazepine resistance in status epilepticus. In our patient population, the optimum threshold for discriminating between benzodiazepine resistant versus sensitive patients was 61 min of seizure activity.

Given the clinical importance of this phenomenon, and our observation that diverse brain insults causing prolonged seizures can all result in benzodiazepine resistance, we used the $0 \, Mg^{2+}$ *in vitro* model of status epilepticus to identify multiple changes in GABAergic signalling that could explain the progressive loss of diazepam efficacy in this condition. Status epilepticus-like activity was accompanied by a modest reduction in GABA synaptic conductance and persistent changes in the efficacy of $Cl^-$ extrusion. However, our major observation was profound short-term, activity-dependent $Cl^-$ accumulation during status epilepticus-like activity. As a result, optogenetic activation of GABAergic interneurons was ineffective at reducing epileptiform activity; on the contrary, GABAergic interneuron firing actually enhanced epileptiform discharges during status epilepticus via excitatory $GABA_AR$ mediated synaptic transmission. This activity-dependent effect is supplemental to two other changes we document, namely the reduced KCC2 expression, and the associated shift in baseline $E_{GABA}$. Together, these results demonstrate why benzodiazepines may fail to enhance inhibition in continuously seizing brain circuits.

The withdrawal of $Mg^{2+}$ *in vitro* has long been used as a model for studying putative changes in GABAergic signalling during status epilepticus (Dreier and Heinemann, 1991; Goodkin *et al.*, 2005; Albus *et al.*, 2008). Dreier *et al.* (1998) were the first to demonstrate that benzodiazepines lose their antiseizure efficacy following the onset of the status epilepticus-like LRD phase in the $0 \, Mg^{2+}$ model. We extend this work by demonstrating that during status epilepticus-like activity, not only do benzodiazepines lose their antiseizure action, but further, they can even exacerbate seizure-like activity. We suggest that the effects of diazepam during status epilepticus we observe are not explained by previously-described deficits in $GABA_AR$ trafficking on principal cells alone (Goodkin *et al.*, 2008), but also by a transient collapse in the transmembrane $Cl^-$ gradient and $E_{GABA}$.

Previous reports suggest that on-going seizure activity results in reduced surface expression, and function, of the

---

**Figure 8 Continued**

$-40 \, mV$ with 100 ms blue light pulses delivered once every 7 s. $t_1$ is a 60 s window of activity, which is expanded in **C** showing epileptiform discharges reliably initiated by optogenetic activation of GAD2+ interneurons. $t_2$ (grey) demarcates section of trace used for analysis. **(D)** Population data from seven slices. *Left* axis (black, histograms with $\pm$ SEM) represents the probability of a discharge being initiated in any given 200 ms time bin within a 7-s window from a 5-min LRD analysis period. Light blue highlights the time bin where light was delivered 3.5 s into the 7-s window. The *right* axis (blue, line plot with $\pm$ SEM) represents the probability of a discharge being present. **(E)** Trace showing a 10-min window from the onset of LRD. $t_1$ and $t_2$ are 60-s periods of activity before and after blue light was delivered as in **B**. $t_3$ and $t_4$ (pink) demarcates section of trace used for analysis in **G** and **H**. **(F)** Expanded $t_1$ and $t_2$ showing 100 ms blue light application (blue bars) reliably initiating discharges. **(G)** Population data ($n = 7$) as in **D** from 5-min analysis periods during LRD prior to light activation. **(H)** Same analysis as in **G** for 5-min analysis periods from the same slices where 100 ms blue light was delivered 3.5 s into every 7-s window. **(I)** Discharge probability significantly increased in the time window where blue light was applied (increased from mean $0.1 \pm$ SEM 0.02 before the light pulses were delivered to mean $0.5 \pm$ SEM 0.1 after light was delivered, $P = 0.002$, paired *t*-test). **(J)** Ten-minute window from the onset of LRD with light-stimulus delivered every 7 s. After at least 5 min of LRD activity, picrotoxin (100 µM) was applied. $t_1$ and $t_2$ are 60-s periods of activity before and after picrotoxin (orange) application. $t_3$ and $t_4$ (pink) demarcates section of trace used for analysis in **L** and **M**. **(K)** Expanded views of $t_1$ and $t_2$ demonstrating that light delivery (blue bars) no longer elicited discharges. **(L)** Population data ($n = 6$) as in **D** from the 5-min analysis window prior to picrotoxin application. **(M)** Data from the same recordings as in **L** for a 5-min analysis period in the presence of picrotoxin. **(N)** Discharge probability significantly decreased in the time bin following blue light application in the presence of picrotoxin (decreased from median 0.6 IQR 0.5–0.8 to median 0.1 IQR 0.0–0.2 following $GABA_AR$ blockade with picrotoxin, $P = 0.03$, Wilcoxon test). **(O)** Cumulative percentage plot showing the distribution of discharge frequencies across three groups, control with photoactivation (On, blue, $n = 20$), no photoactivation (Off, black, $n = 7$) and photoactivation in the presence of picrotoxin (Px, orange, $n = 6$). Grey lines marke x1 and x2 the frequency of the light stimulus (0.14 Hz and 0.28 Hz). **(P)** Population data of discharge frequencies. **(Q)** The difference between frequency of photoactivation (x1 grey line in **O**) and the observed frequency of discharges within a 5-min analysis window. In the on group, this difference was significantly smaller compared to the off and pictrotoxin groups (on: median 0.01 IQR 0.01–0.1Hz versus off: median 0.1 IQR 0.1–0.2Hz, $P = 0.03$, Mann-Whitney U-test and versus pictrotoxin: median 0.1 IQR 0.1–0.2Hz, $P = 0.01$, Mann-Whitney U-test). $^*P \leqslant 0.05$; $^{**}P \leqslant 0.01$; error bars indicate mean $\pm$ SEM.

canonical Cl⁻ extruder KCC2 (Rivera *et al.*, 2004). There are multiple mechanisms by which this could occur including enhanced NMDAR activation, which is known to downregulate KCC2 function (Lee *et al.*, 2011). This is unlikely to result purely from 0 $Mg^{2+}$ treatment as prolonged seizure activity induced by 4-aminopyridine also reduces KCC2 function (Rivera *et al.*, 2004). KCC2 ensures that Cl⁻ is maintained at levels lower than would be predicted by passive processes and also ameliorates activity-dependent Cl⁻ loading (Düsterwald *et al.*, 2018). Loss of KCC2, therefore, constitutes a double blow to the system, since it will cause a rise in baseline intraneuronal [Cl⁻], and reduce the rate of clearance of Cl⁻ , meaning that activity-dependent Cl⁻ loading is exacerbated. We have shown both effects are important. Our findings confirm that the progression to status epilepticus-like activity in the 0 $Mg^{2+}$ model is accompanied by a reduction in KCC2 surface expression and function as evidenced by a progressive depolarization of resting $E_{GABA}$ prior to and following status epilepticus-like activity. In neonatal tissue, ongoing seizure activity is associated with enhanced activity of the Cl⁻ importer NKCC1 (Dzhala *et al.*, 2010). In our preparation, where Cl⁻ homeostasis mechanisms have matured, pharmacological blockade of NKCC1 did not appear to rescue the antiseizure effect of diazepam on status epilepticus-like activity. This suggests that NKCC1 is unlikely to contribute to the Cl⁻ loading we observe. This supports the importance of short-term, activity-dependent, increases in Cl⁻, likely via GABA_ARs themselves (Raimondo *et al.*, 2015). These have been demonstrated previously during single SLEs both *in vitro* and *in vivo* (Isomura *et al.*, 2003; Ellender *et al.*, 2014; Sato *et al.*, 2017), but our new data represent the first time this has been shown to be a factor in persistent status epilepticus-like activity. Our gramicidin perforated patch-clamp recordings and Cl⁻ imaging measurements using the genetically-encoded ratiometric reporter ClopHensorN demonstrate that both single SLEs and status epilepticus-like activity result in substantial intracellular Cl⁻ accumulation and an excitatory shift in $E_{GABA}$. Whether Cl⁻ dysregulation itself drives the transition to status epilepticus-activity or is a product of status epilepticus-activity is still an open question. However, it is worth noting that reducing the function of KCC2 has been shown to accelerate the transition to status epilepticus both *in vitro* (Kelley *et al.*, 2016) and *in vivo* (Silayeva *et al.*, 2015).

Seizures are able to start and spread because of a loss of inhibitory synaptic mechanisms that are typically recruited to 'restrain' excitability within brain circuits (Trevelyan *et al.*, 2006, 2007; Trevelyan and Schevon, 2013). Ongoing failure of inhibitory restraint also underlies the ability of seizures to perpetuate in time and space. Inhibitory restraint can fail due to reduced GABA release (Zhang *et al.*, 2012), GABA_AR internalization (Goodkin *et al.*, 2005), a depolarizing shift in pyramidal $E_{GABA}$ (Lillis *et al.*, 2012) or GABAergic interneurons entering a state of depolarization block (Ziburkus *et al.*, 2006; Cammarota

*et al.*, 2013). Knowing which of these mechanisms are involved in status epilepticus, and to what extent, will be important for designing optimal strategies for aborting seizures, especially given recent interest in using optogenetic strategies to enhance the action of GABAergic interneurons (Krook-Magnuson *et al.*, 2013; Krook-Magnuson and Soltesz, 2015). Using dual whole-cell patch-clamp recordings, we found a high correlation between hippocampal GABAergic interneuronal and pyramidal cell activity during the LRD phase. Optogenetic activation of the pan-interneuronal population using ChR2 expression driven by the GAD2 promoter revealed that activation of GABAergic interneurons has a broadly similar effect on epileptiform activity as diazepam in our model. Interneurons are inhibitory prior to SLEs and excitatory during status epilepticus-like activity. We found that optical activation of the pan-interneuronal population was sufficient to entrain the frequency of epileptiform discharges to the frequency of light activation during the status epilepticus-like phase, and that this entrainment is dependent on intact synaptic transmission via GABA_ARs. This provides strong evidence about three key aspects of interneuronal function during the early stages of status epilepticus: that GABAergic interneurons are able to release GABA, they are not in depolarizing block, and sufficient postsynaptic GABA_ARs are present to mediate GABAergic synaptic transmission. However, because of the transient and widespread collapse of the postsynaptic Cl⁻ gradient in pyramidal neurons, GABAergic interneurons are ineffective at curtailing epileptiform discharges, and in fact drive the generation of these events during status epilepticus-like activity. Our data complement recent *in vitro* and *in vivo* results, which suggest that various GABAergic interneuronal subtypes may promote the extension of seizures when activated once epileptiform activity has become established (Ellender *et al.*, 2014; Sato *et al.*, 2017; Magloire *et al.*, 2019).

Our observation of excitatory GABA_AR-mediated signalling during the LRD phase explains the loss of inhibitory efficacy and the pro-epileptiform effects of diazepam and the low concentration of phenobarbital we observed during the LRD phase. This supports prior work in dissociated cell cultures that demonstrated that activity-driven changes in the Cl⁻ gradient reduce the inhibitory efficacy of diazepam (Deeb *et al.*, 2013). Together, this suggests that benzodiazepines and low concentrations of barbiturates can lose their efficacy in status epilepticus even with GABA_ARs intact. Interestingly we observed that at high concentrations phenobarbital is able to attenuate and abort status epilepticus-like activity. This is likely due to the additional antagonistic effect of high concentrations of phenobarbital on glutamatergic responses via blockade of AMPA and kainate receptors (Macdonald and Barker, 1978; Ko *et al.*, 1997; Meldrum and Rogawski, 2007; Nardou *et al.*, 2011).

Given our experimental findings, it is worth considering why benzodiazepines are often effective in terminating status epilepticus in patients (in our study 52% of patients with status epilepticus responded to benzodiazepine

administration). Brain slices represent a relatively small, well-connected brain circuit, where most areas of the slice are typically involved in status epilepticus-like activity (Ellender *et al.*, 2014). This means that most pyramidal cells in the slice may experience an activity-dependent collapse of the $Cl^-$ gradient, which will render benzodiazepines ineffective during prolonged seizures. In patients with status epilepticus, the situation is likely to be different. The proportion of brain circuits affected by activity-dependent $Cl^-$ accumulation will vary considerably between patients depending on the seizure type as well as the extent to which different brain areas are recruited into the seizure process. Interactions between areas may also be critical in providing pacemaker drives (Codadu *et al.*, 2019), thereby maintaining a high rate of discharge, but breaking this loop by slightly reducing the intrinsic rate at a particular site may be all that is required. In regions where intracellular $Cl^-$ and $E_{GABA}$ are still low, benzodiazepines will enhance inhibitory restraint. Therefore, determining the potential cumulative effect of benzodiazepines may involve a dynamic contest between areas where it enhances inhibition and those areas where it is ineffective or promotes hyperexcitability.

Given the demonstrated potential for benzodiazepines to be ineffective, or even promote seizure prolongation in status epilepticus, we recommend investigation of alternative or adjunctive therapeutic strategies for terminating status epilepticus. These could involve strategies for enhancing $Cl^-$ extrusion capacity to help maintain $E_{GABA}$ (Gagnon *et al.*, 2013; Alfonsa *et al.*, 2016; Moore *et al.*, 2017; Magloire *et al.*, 2019), or targeting of other brain inhibitory systems including modulating pH (Tolner *et al.*, 2011), postsynaptic $K^+$ conductance (Zhang *et al.*, 2017) or glutamatergic transmission. Our work supports the use of agents that target multiple receptor systems for aborting seizure activity, such as the barbiturate phenobarbital. Given that total duration in status is correlated with morbidity, and that phenobarbital at sufficiently high dosage is highly effective at aborting status epilepticus (Burman *et al.*, 2019), we suggest that phenobarbital be re-evaluated as a first-line agent in status epilepticus. This is particularly the case as long-term cognitive side effects of one-off phenobarbital use have not been demonstrated.

In summary, our findings support the idea that dynamic network changes and ionic mechanisms likely contribute to the development of persistent seizure activity and that an enhanced understanding of these alterations will guide the development of more effective strategies for treating status epilepticus.

## Acknowledgements

## Funding

## Competing interests

The authors report no competing interests.

## Supplementary material

Supplementary material is available at *Brain* online.

## References

Albus K, Wahab A, Heinemann U. Standard antiepileptic drugs fail to block epileptiform activity in rat organotypic hippocampal slice cultures. Br J Pharmacol 2008; 154: 709–24.

Alfonsa H, Lakey JH, Lightowlers RN, Trevelyan AJ. Cl-out is a novel cooperative optogenetic tool for extruding chloride from neurons. Nat Commun 2016; 7: 13495.

Alger B, Nicoll R. GABA-mediated biphasic inhibitory responses in hippocampus. Nature 1979; 281: 315.

Anderson WW, Lewis DV, Swartzwelder HS, Wilson WA. Magnesium-free medium activates seizure-like events in the rat hippocampal slice. Brain Res 1986; 398: 215–9.

Appleton R, Choonara I, Martland T, Phillips B, Scott R, Whitehouse W, et al. The treatment of convulsive status epilepticus in children. Arch Dis Childhood 2000; 83: 415–9.

Arosio D, Ricci F, Marchetti L, Gualdani R, Albertazzi L, Beltram F. Simultaneous intracellular chloride and pH measurements using a GFP-based sensor. Nat Methods 2010; 7: 516.

Boggs JG. Mortality associated with status epilepticus. Epilepsy Currents 2004; 4: 25–7.

Burman RJ, Ackerman S, Shapson-Coe A, Ndondo A, Buys H, Wilmshurst JM. A comparison of parenteral phenobarbital versus parenteral phenytoin as second-line management for paediatric convulsive status epilepticus in a resource-limited setting. Front Neurol 2019; 10: 506.

Cammarota M, Losi G, Chiavegato A, Zonta M, Carmignoto G. Fast spiking interneuron control of seizure propagation in a cortical slice model of focal epilepsy. J Physiol 2013; 591: 807–22.

Chin RF, Neville BG, Peckham C, Wade A, Bedford H, Scott RC. Treatment of community-onset, childhood convulsive status

epilepticus: a prospective, population-based study. Lancet Neurol 2008; 7: 696–703.

Codadu NK, Parrish RR, Trevelyan AJ. Region-specific differences and areal interactions underlying transitions in epileptiform activity. J Physiol 2019; 597: 2079–96.

Deeb TZ, Maguire J, Moss SJ. Possible alterations in GABAA receptor signaling that underlie benzodiazepine-resistant seizures. Epilepsia 2012; 53: 79–88.

Deeb TZ, Nakamura Y, Frost GD, Davies PA, Moss SJ. Disrupted Cl– homeostasis contributes to reductions in the inhibitory efficacy of diazepam during hyperexcited states. Eur J Neurosci 2013; 38: 2453–67.

Dreier J, Heinemann U. Regional and time dependent variations of low Mg 2+ induced epileptiform activity in rat temporal cortex slices. Exp Brain Res 1991; 87: 581–96.

Dreier J, Zhang CL, Heinemann U. Phenytoin, phenobarbital, and midazolam fail to stop status epilepticus-like activity induced by low magnesium in rat entorhinal slices, but can prevent its development. Acta Neurol Scand 1998; 98: 154–60.

Düsterwald KM, Currin CB, Burman RJ, Akerman CJ, Kay AR, Raimondo JV. Biophysical models reveal the relative importance of transporter proteins and impermeant anions in chloride homeostasis. eLife 2018; 7: e39575.

Dzhala VI, Kuchibhotla KV, Glykys JC, Kahle KT, Swiercz WB, Feng G, et al. Progressive NKCC1-dependent neuronal chloride accumulation during neonatal seizures. J Neurosci 2010; 30: 11745–61.

Ellender TJ, Raimondo JV, Irkle A, Lamsa KP, Akerman CJ. Excitatory effects of parvalbumin-expressing interneurons maintain hippocampal epileptiform activity via synchronous afterdischarges. J Neurosci 2014; 34: 15208–22.

Fernández IS, Abend NS, Agadi S, An S, Arya R, Brenton JN, et al. Time from convulsive status epilepticus onset to anticonvulsant administration in children. Neurology 2015; 84: 2304–11.

Fujiwara-Tsukamoto Y, Isomura Y, Imanishi M, Ninomiya T, Tsukada M, Yanagawa Y, et al. Prototypic seizure activity driven by mature hippocampal fast-spiking interneurons. J Neurosci 2010; 30: 13679–89.

Gagnon M, Bergeron MJ, Lavertu G, Castonguay A, Tripathy S, Bonin RP, et al. Chloride extrusion enhancers as novel therapeutics for neurological diseases. Nat Med 2013; 19: 1524.

Gaínza-Lein M, Fernández IS, Jackson M, Abend NS, Arya R, Brenton JN, et al. Association of time to treatment with short-term outcomes for pediatric patients with refractory convulsive status epilepticus. JAMA Neurol 2018; 75: 410–8.

Gaínza-Lein M, Fernández IS, Ulate-Campos A, Loddenkemper T, Ostendorf AP. Timing in the treatment of status epilepticus: from basics to the clinic. Seizure 2019; 68: 22–30.

Glauser T, Shinnar S, Gloss D, Alldredge B, Arya R, Bainbridge J, et al. Evidence-based guideline: treatment of convulsive status epilepticus in children and adults: report of the Guideline Committee of the American Epilepsy Society. Epilepsy Curr 2016; 16: 48–61.

Goodkin HP, Joshi S, Mtchedlishvili Z, Brar J, Kapur J. Subunit-specific trafficking of GABAA receptors during status epilepticus. J Neurosci 2008; 28: 2527–38.

Goodkin HP, Kapur J. The impact of diazepam's discovery on the treatment and understanding of status epilepticus. Epilepsia 2009; 50: 2011–8.

Goodkin HP, Yeh J-L, Kapur J. Status epilepticus increases the intracellular accumulation of GABAA receptors. J Neurosci 2005; 25: 5511–20.

Gutiérrez R, Heinemann U. Synaptic reorganization in explanted cultures of rat hippocampus. Brain Res 1999; 815: 304–16.

Ilie A, Raimondo JV, Akerman CJ. Adenosine release during seizures attenuates GABAA receptor-mediated depolarization. J Neurosci 2012; 32: 5321–32.

Isomura Y, Sugimoto M, Fujiwara-Tsukamoto Y, Yamamoto-Muraki S, Yamada J, Fukuda A. Synaptically activated Cl–accumulation responsible for depolarizing GABAergic responses in mature hippocampal neurons. J Neurophysiol 2003; 90: 2752–6.

Jiruska P, De Curtis M, Jefferys JG, Schevon CA, Schiff SJ, Schindler K. Synchronization and desynchronization in epilepsy: controversies and hypotheses. J Physiol 2013; 591: 787–97.

Kaila K, Pasternack M, Saarikoski J, Voipio J. Influence of GABA-gated bicarbonate conductance on potential, current and intracellular chloride in crayfish muscle fibres. J Physiol 1989; 416: 161–81.

Kamphuis W, Gorter J, Da Silva FL. A long-lasting decrease in the inhibitory effect of GABA on glutamate responses of hippocampal pyramidal neurons induced by kindling epileptogenesis. Neuroscience 1991; 41: 425–31.

Kapur J, Coulter DA. Experimental status epilepticus alters γ-aminobutyric acid type A receptor function in CA1 pyramidal neurons. Ann Neurol 1995; 38: 893–900.

Kelley MR, Deeb TZ, Brandon NJ, Dunlop J, Davies PA, Moss SJ. Compromising KCC2 transporter activity enhances the development of continuous seizure activity. Neuropharmacology 2016; 108: 103–10.

Khoshkhoo S, Vogt D, Sohal VS. Dynamic, cell-type-specific roles for GABAergic interneurons in a mouse model of optogenetically inducible seizures. Neuron 2017; 93: 291–8.

Ko GY-PL, Brown-Croyts LM, Teyler TJ. The effects of anticonvulsant drugs on NMDA-EPSP, AMPA-EPSP, and GABA-IPSP in the rat hippocampus. Brain Res Bull 1997; 42: 297–302.

Krook-Magnuson E, Armstrong C, Oijala M, Soltesz I. On-demand optogenetic control of spontaneous seizures in temporal lobe epilepsy. Nat Commun 2013; 4: 1376.

Krook-Magnuson E, Soltesz I. Beyond the hammer and the scalpel: selective circuit control for the epilepsies. Nat Neurosci 2015; 18: 331.

Kyrozis A, Reichling DB. Perforated-patch recording with gramicidin avoids artifactual changes in intracellular chloride concentration. J Neurosci Methods 1995; 57: 27–35.

Lamsa K, Kaila K. Ionic mechanisms of spontaneous GABAergic events in rat hippocampal slices exposed to 4-aminopyridine. J Neurophysiol 1997; 78: 2582–91.

Lee HH, Deeb TZ, Walker JA, Davies PA, Moss SJ. NMDA receptor activity downregulates KCC2 resulting in depolarizing GABA A receptor–mediated currents. Nat Neurosci 2011; 14: 736.

Lillis KP, Kramer MA, Mertz J, Staley KJ, White JA. Pyramidal cells accumulate chloride at seizure onset. Neurobiol Dis 2012; 47: 358–66.

Macdonald RL, Barker JL. Different actions of anticonvulsant and anesthetic barbiturates revealed by use of cultured mammalian neurons. Science 1978; 200: 775–7.

Magloire V, Cornford J, Lieb A, Kullmann DM, Pavlov I. KCC2 overexpression prevents the paradoxical seizure-promoting action of somatic inhibition. Nat Commun 2019; 10: 1225.

Mann EO, Kohl MM, Paulsen O. Distinct roles of GABAA and GABAB receptors in balancing and terminating persistent cortical activity. J Neurosci 2009; 29: 7513–8.

Mayer SA, Claassen J, Lokin J, Mendelsohn F, Dennis LJ, Fitzsimmons B-F. Refractory status epilepticus: frequency, risk factors, and impact on outcome. Arch Neurol 2002; 59: 205–10.

Meldrum BS, Rogawski MA. Molecular targets for antiepileptic drug development. Neurotherapeutics 2007; 4: 18–61.

Mody I, Lambert J, Heinemann U. Low extracellular magnesium induces epileptiform activity and spreading depression in rat hippocampal slices. J Neurophysiol 1987; 57: 869–88.

Moore YE, Kelley MR, Brandon NJ, Deeb TZ, Moss SJ. Seizing control of KCC2: a new therapeutic target for epilepsy. Trends Neurosci 2017; 40: 555–71.

Morimoto K, Fahnestock M, Racine RJ. Kindling and status epilepticus models of epilepsy: rewiring the brain. Progr Neurobiol 2004; 73: 1–60.

Nardou R, Yamamoto S, Bhar A, Burnashev N, Ben-Ari Y, Khalilov I. Phenobarbital but not diazepam reduces AMPA/kainate receptor

mediated currents and exerts opposite actions on initial seizures in the neonatal rat hippocampus. Front Cell Neurosci 2011; 5: 16.

Naylor DE. Treating acute seizures with benzodiazepines: does seizure duration matter? Epileptic Disorders 2014; 16: 69–83.

Naylor DE, Liu H, Wasterlain CG. Trafficking of GABAA receptors, loss of inhibition, and a mechanism for pharmacoresistance in status epilepticus. J Neurosci 2005; 25: 7724–33.

Raimondo JV, Burman RJ, Katz AA, Akerman CJ. Ion dynamics during seizures. Front Cell Neurosci 2015; 9: 419.

Raimondo JV, Joyce B, Kay L, Schlagheck T, Newey SE, Srinivas S, et al. A genetically-encoded chloride and pH sensor for dissociating ion dynamics in the nervous system. Front Cell Neurosci 2013; 7: 202.

Raimondo JV, Kay L, Ellender TJ, Akerman CJ. Optogenetic silencing strategies differ in their effects on inhibitory synaptic transmission. Nat Neurosci 2012; 15: 1102.

Raimondo JV, Tomes H, Irkle A, Kay L, Kellaway L, Markram H, et al. Tight coupling of astrocyte pH dynamics to epileptiform activity revealed by genetically encoded pH sensors. J Neurosci 2016; 36: 7002–13.

Rivera C, Voipio J, Thomas-Crusells J, Li H, Emri Z, Sipilä S, et al. Mechanism of activity-dependent downregulation of the neuron-specific K-Cl cotransporter KCC2. J Neurosci 2004; 24: 4683–91.

Royo NC, Vandenberghe LH, Ma J-Y, Hauspurg A, Yu L, Maronski M, et al. Specific AAV serotypes stably transduce primary hippocampal and cortical cultures with high efficiency and low toxicity. Brain Res 2008; 1190: 15–22.

Sato SS, Artoni P, Landi S, Cozzolino O, Parra R, Pracucci E, et al. Simultaneous two-photon imaging of intracellular chloride concentration and pH in mouse pyramidal neurons in vivo. Proc Natl Acad Sci 2017; 114: E8770–E9.

Silayeva L, Deeb TZ, Hines RM, Kelley MR, Munoz MB, Lee HH, et al. KCC2 activity is critical in limiting the onset and severity of status epilepticus. Proc Natl Acad Sci 2015; 112: 3523–28.

Staley KJ, Soldo BL, Proctor WR. Ionic mechanisms of neuronal excitation by inhibitory GABAA receptors. Science 1995; 269: 977–81.

Stoppini L, Buchs P-A, Muller D. A simple method for organotypic cultures of nervous tissue. J Neurosci Methods 1991; 37: 173–82.

Swartzwelder HS, Lewis D, Anderson W, Wilson W. Seizure-like events in brain slices: suppression by interictal activity. Brain Res 1987; 410: 362–6.

Taniguchi H, He M, Wu P, Kim S, Paik R, Sugino K, et al. A resource of Cre driver lines for genetic targeting of GABAergic neurons in cerebral cortex. Neuron 2011; 71: 995–1013.

Tolner EA, Hochman DW, Hassinen P, Otáhal J, Gaily E, Haglund MM, et al. Five percent CO2 is a potent, fast-acting inhalation anticonvulsant. Epilepsia 2011; 52: 104–14.

Trevelyan AJ, Schevon CA. How inhibition influences seizure propagation. Neuropharmacology 2013; 69: 45–54.

Trevelyan AJ, Sussillo D, Watson BO, Yuste R. Modular propagation of epileptiform activity: evidence for an inhibitory veto in neocortex. J Neurosci 2006; 26: 12447–55.

Trevelyan AJ, Sussillo D, Yuste R. Feedforward inhibition contributes to the control of epileptiform propagation speed. J Neurosci 2007; 27: 3383–7.

Trinka E, Cock H, Hesdorffer D, Rossetti AO, Scheffer IE, Shinnar S, et al. A definition and classification of status epilepticus–Report of the ILAE Task Force on Classification of Status Epilepticus. Epilepsia 2015; 56: 1515–23.

Wright R, Newey SE, Ilie A, Wefelmeyer W, Raimondo JV, Ginham R, et al. Neuronal chloride regulation via KCC2 is modulated through a GABAB receptor protein complex. J Neurosci 2017: 2164–16.

Wright R, Raimondo J, Akerman C. Spatial and temporal dynamics in the ionic driving force for GABAA receptors. Neural Plasticity 2011; 2011: 728395.

Zhang CL, Dreier JP, Heinemann U. Paroxysmal epileptiform discharges in temporal lobe slices after prolonged exposure to low magnesium are resistant to clinically used anticonvulsants. Epilepsy research 1995; 20: 105–11.

Zhang T, Todorovic MS, Williamson J, Kapur J. Flupirtine and diazepam combination terminates established status epilepticus: results in three rodent models. Ann Clin Transl Neurol 2017; 4: 888–96.

Zhang ZJ, Koifman J, Shin DS, Ye H, Florez CM, Zhang L, et al. Transition to seizure: ictal discharge is preceded by exhausted presynaptic GABA release in the hippocampal CA3 region. J Neurosci 2012; 32: 2499–512.

Ziburkus J, Cressman JR, Barreto E, Schiff SJ. Interneuron and pyramidal cell interplay during in vitro seizure-like events. J Neurophysiol 2006; 95: 3948–54.